

INVESTIGATION OF HIGH STRAIN RATE PROPERTIES
OF GRAPHENE REINFORCED ALUMINUM FOAM
UNDER VARYING TEMPERATURE

A Thesis
presented to
the Faculty of the Graduate School
at the University of Missouri-Columbia

In Partial Fulfillment
of the Requirements for the Degree
Master of Science

By
AKHOURI AMITANAND SINHA
Dr. Sanjeev Khanna, Thesis Supervisor

JULY 2018

The undersigned, appointed by the dean of the Graduate School, have examined the thesis entitled

INVESTIGATION OF HIGH STRAIN RATE PROPERTIES
OF GRAPHENE REINFORCED ALUMINUM FOAM
UNDER VARYING TEMPERATURE

Presented by Akhouri Amitanand Sinha,

A candidate for the degree of Master of Science,

And hereby certify that, in their opinion, it is worthy of acceptance

Dr. Sanjeev Khanna

Dr. Jacob McFarland

Dr. Sarah Orton

ACKNOWLEDGMENTS

I would like to express my gratitude to my advisor, Dr. Sanjeev Khanna, for his kind mentorship and endless support for my research. Dr. Khanna supported me with ideas related to engineering and guided me throughout the duration of my research.

I would like to thank my thesis committee, Dr. Jacob McFarland and Dr. Sarah Orton for their insightful comments. I would like to thank my parents for constantly supporting and motivating me to always do my best. I would like to thank all my friends for encouraging me to always challenge myself and keep getting better.

TABLE OF CONTENTS

ACKNOWLEDGMENTS	ii
LIST OF TABLES	vii
LIST OF FIGURES	viii
ABSTRACT.....	x
CHAPTER ONE: INTRODUCTION.....	1
1.1 Introduction	1
1.2 Properties of Aluminum Foam	2
1.3 Properties of Graphene (GR).....	3
1.4 Split Hopkinson pressure bar (SHPB).....	4
1.5 Dynamic compression at high temperature	7
1.6 Applications	9
1.7 Objective of this work.....	14
1.8 Layout of this thesis	15
CHAPTER TWO: EXPERIMENTAL METHODS	16
2.1 Split Hopkinson Pressure Bar (SHPB) theory.....	16
2.2 Assumptions of a valid SHPB test	19
2.3 Experimental Set up	19

2.3.1 Gas launcher assembly	21
2.3.2 Pressure bar assembly.....	22
2.3.3 Data acquisition system	26
2.4 Working principle	31
2.5 Calibration.....	32
2.6 Graphene reinforced Aluminum foam fabrication	37
2.7 Pulse shaping technique	39
2.8 Effect of strain rate at high temperature.....	43
2.9 Data analysis	44
CHAPTER THREE: HIGH STRAIN RATE PROPERTIES	47
OF GRAPHENE REINFORCED ALUMINUM FOAMS.....	47
AT ROOM TEMPERATURE	47
CHAPTER FOUR: HIGH STRAIN RATE PROPERTIES	54
OF GRAPHENE REINFORCED ALUMINUM FOAMS.....	54
AT HIGH TEMPERATURE	54
CHAPTER FIVE: CONCLUSION.....	67
REFERENCES	69

LIST OF TABLES

Table	Page no.
Table 2.1 Properties of SHPB components.....	24
Table 2.2 Strain correction factors for incident and transmitted bars.....	35
Table 2.3 Stress correction factors.....	36
Table 2.4 Properties of Tellurium copper pulse shaper.....	40
Table 3.1 Peak and plateau stresses at different strain rates and graphene composition.....	52
Table 4.1 Peak and plateau stresses at different strain rates and graphene composition at 473K.....	64
Table 4.2 Peak and plateau stresses at different strain rates and graphene composition at 623 K.....	65

LIST OF FIGURES

Figure	Page no.
Figure 1.1 A view of graphene monolayer.....	3
Figure 1.2 Influence of strain rate on plateau stress of al-foams for various densities.....	6
Figure 1.3 Stress-strain plot at various temperatures.....	8
Figure 1.4 Applications of aluminum foams in various industries.....	10
Figure 1.5 Application of Al-foams in high speed trains as a replacement of GFRP.....	11
Figure 1.6 Application of Al-foams in high speed trains as a replacement of GFRP.....	11
Figure 1.7 Application of Al-foams in high speed trains as a replacement of GFRP.....	12
Figure 1.8 Aluminum foam used in car body structures.....	12
Figure 1.9 Vacuum lifting tool made of Al-foam.....	13
Figure 1.10 Al-foam used in crash box.....	13
Figure 2.1 Schematic description of SHPB.....	16
Figure 2.2 Schematic diagram of SHPB system.....	20
Figure 2.3 Gas launch assembly of in-house SHPB apparatus.....	22
Figure 2.4 Aluminum striker bar with 457.2 mm in length and 12.7 mm in diameter.....	23
Figure 2.5 Incident bar in the SHPB apparatus.....	25
Figure 2.6 Transmitted bar in the SHPB apparatus.....	25
Figure 2.6 Damping system.....	26
Figure 2.7 A quarter bridge strain gage circuit.....	27
Figure 2.8 A measured incident and reflected pulse.....	28
Figure 2.8 A measured transmitted pulse.....	28
Figure 2.9 Differential preamplifiers and PXI system.....	29
Figure 2.10 LabVIEW interface.....	30

Figure 2.11 Experimental constants in LabVIEW interface.....	30
Figure 2.12 Pulse shaper, striker bar and incident bar.....	31
Figure 2.13 An overview of in-house SHPB system.....	32
Figure 2.14 Low speed diamond wheel saw.....	38
Figure 2.15 Specimen used in SHPB testing.....	38
Figure 2.16 A five hole pulse shaper.....	40
Figure 2.17 Stress equilibrium without pulse shaper.....	41
Figure 2.18 Stress equilibrium with the use of five holed pulse shaper.....	41
Figure 2.19 Strain rate without pulse shaper.....	42
Figure 2.20 Strain rate with pulse shaper.....	42
Figure 2.21 Setup of high temperature in SHPB system.....	43
Figure 2.22 SHPB data in Excel before modifying.....	44
Figure 2.23 SHPB data after modifying.....	45
Figure 2.24 Incident and transmitted signal graphs	46
Figure 3.1 Typical compressive stress-strain behavior of aluminum foam.....	47
Figure 3.2 High strain rate (1000 s^{-1}) compressive stress-strain response for different graphene composition.....	49
Figure 3.3 High strain rate (1400 s^{-1}) compressive stress-strain response for different graphene composition.....	49
Figure 3.4 High strain rate (1800 s^{-1}) compressive stress-strain response for different graphene composition.....	50
Figure 3.5 High strain rate (2200 s^{-1}) compressive stress-strain response for different graphene composition.....	51
Figure 3.6 Energy absorption of aluminum foams as a function of strain rates.....	53
Figure 4.1 High strain rate (1000 s^{-1}) response of aluminum foams reinforced with various graphene compositions (a) 0.2 wt.%, (b) 0.4wt.%, (c) 0.5 wt.%, (d) 0.62 wt.%	56
Figure 4.2 High strain rate (1400 s^{-1}) response of aluminum foams reinforced with various graphene compositions (a) 0.2 wt.%, (b) 0.4wt.%, (c) 0.5 wt.%, (d) 0.62 wt.%.....	58

Figure 4.3 High strain rate (1800 s^{-1}) response of aluminum foams reinforced with various graphene compositions (a) 0.2 wt.%, (b) 0.4wt.%, (c) 0.5 wt.%, (d) 0.62 wt.%.....	60
Figure 4.4 High strain rate (2200 s^{-1}) response of aluminum foams reinforced with various graphene compositions (a) 0.2 wt.%, (b) 0.4wt.%, (c) 0.5 wt.%, (d) 0.62 wt.%.....	63
Figure 4.5 Values of peak stress for different compositions of graphene reinforced aluminum foam at different strain rates and temperatures.....	65
Figure 4.6 Values of plateau stress for different compositions of graphene reinforced aluminum foam at different strain rates and temperatures.....	66
Figure 4.7 Values of energy absorption for different compositions of graphene reinforced aluminum foam at different strain rates and temperatures	66

ABSTRACT

Closed cell aluminum foam is a unique type of lightweight metal that is able to sustain considerable deformation under a nearly constant stress known as plateau stress. Under dynamic loading, aluminum foams are good energy absorbers. However, they still suffer from low strength and therefore, it is important to enhance the strength of closed cell aluminum foams. In this investigation, aluminum foams reinforced with different graphene concentrations: 0.2, 0.4, 0.5, 0.62 wt.%. were fabricated using a liquid metallurgy route. The compressive dynamic behavior of Al-foam reinforced with graphene has been studied over a range of strain rate ranging from 1000 s^{-1} to 2200 s^{-1} using the Split Hopkinson Pressure Bar (SHPB) apparatus. The mechanical response was studied at room temperature (298 K) as well as at a high temperature of 473 K and 623 K. It was observed that graphene reinforced aluminum foams are sensitive to strain rate. Mechanical properties like peak stress, plateau stress and energy absorption were examined. Among the different graphene concentrations investigated under various strain rates, 0.62 wt. % aluminum foam showed the highest peak stress, plateau stress and energy absorption over the temperature range studied.

CHAPTER ONE: INTRODUCTION

1.1 Introduction

Aluminum foams are excellent candidates for lightweight engineering structures due to the fact that under compressive loading, they have superb energy absorption capacity. Nonetheless, there is an insufficient amount of work on mechanical properties of closed cell aluminum foams at high strain rates, and more research on this would lead to a better insight of the mechanical properties of aluminum foams under high impact loadings.

When compared with polymeric foams, closed cell aluminum foams have a greater energy absorption capacity but have a relatively low compressive strength. Thus, it is essential to increase the strength of Al foams. This could be achieved with the help of nanomaterials as reinforcements in the foam. Higher strength could result in lower cross sectional dimensions thereby, reducing the overall weight of the system.

In the present investigation, the mechanical property of closed cell aluminum foams reinforced with graphene at high strain rates has been studied. Liquid metallurgy method is used to add graphene to molten aluminum which increases the viscosity and increases the stability of cells during the foaming process. Also, this study comprises of effect of dynamic loading at high temperature (up to 300°C). Furthermore, no work has been found in the field of high strain rate behavior of aluminum foams reinforced with graphene under compressive loading at high temperature, to the best of our knowledge.

1.2 Properties of Aluminum Foam

Metal foams are a unique class of cellular metals that are made by purposely adding pores during fabrication. Even though the initial attempt to fabricate metal foam was in the year 1925 [1], researchers have started to give their attention to metal foams, especially aluminum foams, only in the last two decades. Practical applications of metal foams include energy absorption, vibration and noise reduction in industrial and civil structures [2].

Cellular materials having a distinct periodic configuration e.g. honeycombs are extensively used in the case of dynamic loading. But, when compared with aluminum foams, these materials are more heavy, expensive and anisotropic. Characteristics of aluminum foams include lightweight, high strength to weight ratio, high energy absorption capacity and specific strength. They get these properties because they are able to experience substantial strains under nearly constant stress which is known as plateau stress. But, since they have a low compressive strength, they are generally only used as a core in a layered material [3-5].

There are two types of foams: open cell and closed cell. Open cell foams have cells that are open to each other in a mesh like structure where liquid or gas can pass through. Whereas, in closed cell, the cells are not interconnected with each other. Therefore, the mechanical behavior of the foam under dynamic loading is governed by properties of cell wall and cell morphology [6-8].

1.3 Properties of Graphene (GR)

Graphene (GR) was introduced in the year 2004. It is a rigidly packed two dimensional lattice, of a monolayer of carbon atoms having a honeycomb structure as shown in Figure 1.1.

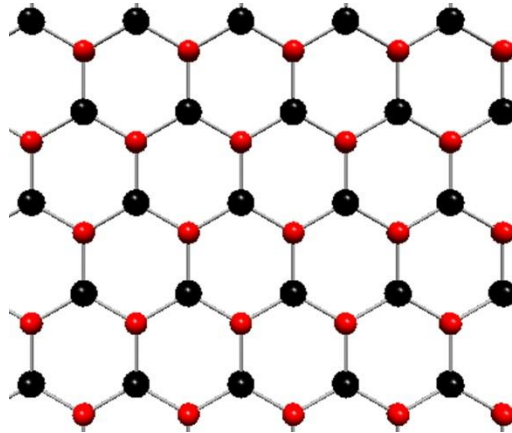


Figure 2.1 A view of graphene monolayer

Graphene is an inexpensive material which is available in substantial amount. It is well known for improving mechanical, thermal and electrical properties of various materials. Research has shown that the breaking strength of GR is 200 times more than that of steel. It has a Young's modulus of 1,060 TPa and a bulk Ultimate strength of 130 GPa. Its thermal conductivity and electrical conductivity are 5000 W/m-k and 6000 S/cm respectively which makes it an ideal material to be used in nanoelectronics [9]. Due to these exceptional properties, GR can be used in numerous applications like batteries, solar cells, super capacitors, sensors and nanocomposites [10].

1.4 Split Hopkinson pressure bar (SHPB)

It is essential to examine the change in mechanical properties of materials with strain rate because material properties can vary significantly with the loading rate. Nowadays, different methods have been developed to investigate mechanical properties at high strain rate loadings. One such technique is the Split Hopkinson Pressure Bar (SHPB). It is generally used to study the response of materials under compression, tension or torsion for strain rates up to $10,000 \text{ s}^{-1}$.

Hopkinson [11] in 1914 measured the effect of induced wave pressure in long elastic metallic bars. He studied the propagation of stress pulse in long metallic rods. In 1949, Kolsky [12] developed upon the research by Hopkinson by sandwiching a sample between two metallic bars and examined the stress-strain behavior of materials at high strain rates.

Mukai *et al.* [13] investigated the effect of high strain rate on Alporas (a particular type of closed cell aluminum foam having a chemical composition of Al-1.42Ca-1.42Ti-0.28Fe-0.007Mg by mass%). They found that Alporas is heavily dependent on strain rates. They also studied that under compressive loading the energy absorption per unit volume of Alporas foam increased by 50% when the strain rate was changed from quasi static to dynamic (over 1000 s^{-1}). They also evaluated the effect of sample height on yield strength and concluded that there was minimal change in the yield strength over a height range of 6-100 mm.

Zhao *et al.* [14] investigated compressive testing at quasi static and high strain rates on two different types of aluminum foams namely, Cymat (manufactured using gas injection process) and IFAM (obtained from aluminum powder through the blowing process that used 0.5 wt.% titanium hydride powder as a blowing agent). They found that Cymat foams do not show strain rate sensitivity due to the fracture of cell walls whereas they observed a 15% enhancement of IFAM foam as the crushing mechanism was fracture of the cell walls.

Frew *et al.* [15] studied the stress-strain response on brittle materials such as glass ceramic. In order to obtain accurate and smoother results, they modified the standard SHPB using an annealed thin C11000 copper disk to obtain stress equilibrium and a constant strain rate over the loading duration.

Hamada *et al.* [16] conducted a competitive study for pure aluminum foam under dynamic and static loadings. They found an increase in the plateau stress at different loadings with an increase in the density. They concluded that, plateau stress increase due to a rise in the inner gas pressure as well as due to the strength of the cell wall and it is 1.3 times larger when it is loaded dynamically.

Gray *et al.* [17] demonstrated the effect of temperature and strain rate on the mechanical properties of Adiprene L-100, a polyether urethane-based rubber. They studied the mechanical behavior of Adiprene between the range of strain rate from 0.001 s^{-1} to 7000 s^{-1} and the temperature range between 77 K to 298 K. Chen *et al.*

[18] presented a new technique to measure the dynamic properties of materials that have low compressive strengths like elastomers by using a modified Split Hopkinson Pressure Bar. They used an aluminum alloy that had a low Young's modulus and was also hollow to reduce the cross sectional area in order to increase the transmitted strain.

Raj *et al.* [19] studied the dependence of relative density (0.06 to 0.4) and strain rate ($1 \cdot 10^{-3} \text{ s}^{-1}$ for quasi static compression and $5 \cdot 10^2 \text{ s}^{-1}$ to $1 \cdot 10^3 \text{ s}^{-1}$ for dynamic loading) on the mechanical behavior of aluminum foams. They found an increase in plateau stress with an increase in relative density and greater strain rate sensitivity was displayed for higher relative density foams. Fig. 1.2 shows the dependence of strain rate on plateau stress. According to them this phenomenon was because the gases entrapped in the closed cell foam provided resistance to deformation and due to geometric softening.

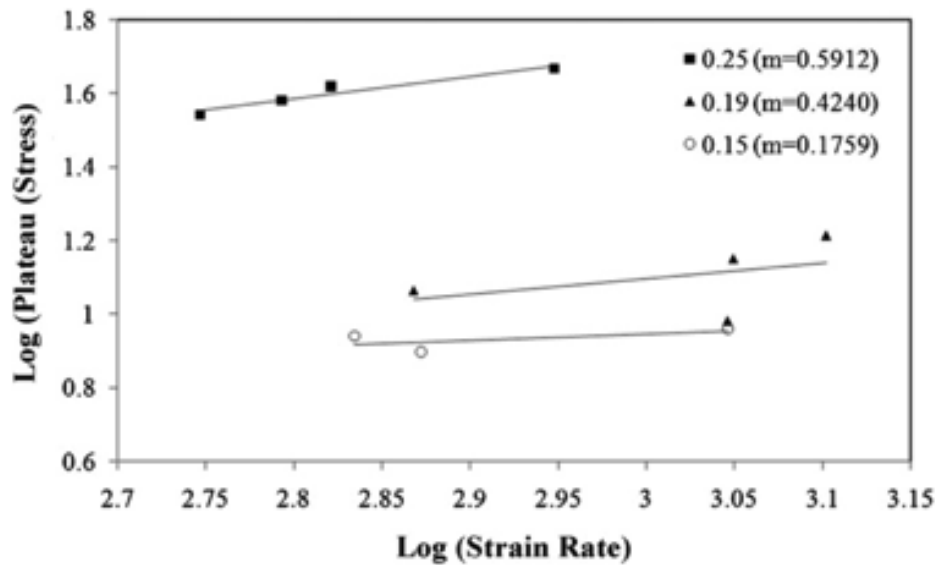


Figure 1.2 Influence of strain rate on plateau stress of al-foams for various densities

1.5 Dynamic compression at high temperature

Hakamada *et al.* [20] inspected the compressive behavior of aluminum foams at a range of high temperature from 573 K to 773 K under quasi static loading and concluded that at high temperature the Al-foam displayed similar deformation mechanism when compared to the bulk reference aluminum (a cell wall material of the aluminum foam).

Aly M. [21] investigated the compressive behavior of Alporas at temperature ranging from 25 °C to 650 °C and under low and high strain rates. They concluded that mechanical properties of Alporas are reliant on density and temperature. Cady *et al.* [22] also studied the behavior of Alporas as a function of temperature and concluded that the compressive stress-strain response of the material was dependent on the temperature.

Wang *et al.* [23] conducted a study on mechanical properties of Al-foams over a range of high temperatures (298 K – 773 K) under both quasi static and dynamic loading as shown in Figure 1.3 using a Split Hopkinson Pressure Bar system. They found that aluminum showed not only strong strain rate sensitivity but also was dependent on temperature. Using the high speed photography they observed that deformation of aluminum foam under dynamic loading is caused due to plastic bending of cell wall at elevated temperatures.

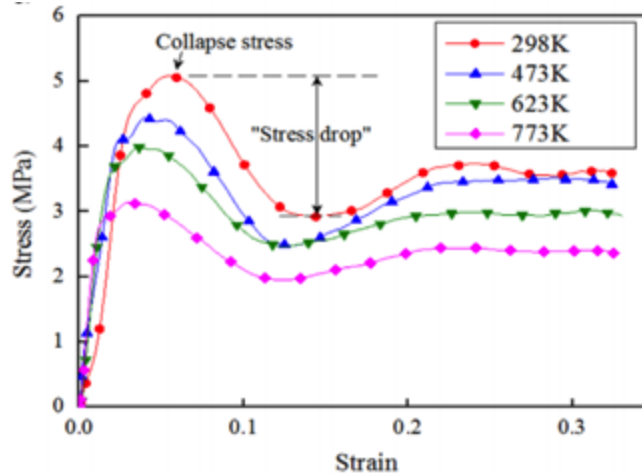


Figure 1.3 Stress-strain plot at various temperatures

It is essential to maintain a constant Young's modulus of the pressure bars in Split Hopkinson Pressure Bar (SHPB) while testing, as they not only serve as medium for transfer of loading wave but also assist as a sensor from which the strain gages measure the incident, reflected and transmitted waves. Since, at high temperature the young's modulus of a material changes, it influences the precision at which the signals are recorded and thereby affecting the calculations [24]. Thus, it must be seen that the incident and transmitted bars are kept at room temperature while heating the specimen. The time in which an independently heated specimen is brought into contact with the cold incident and transmitted bar before applying the load is known as cold contact time (CCT). It is preferable to have a very short CCT. Apostol *et al.* [25] used an automated SHPB for achieving a short CCT whereas Franz *et al.* [26] after heating the sample got the incident and transmitted bar into contact with the specimen and launched the striker bar.

In the current study, the Al-foam is heated using an infrared heater separately to the desired temperature before bringing the bars into contact with the heated specimen and applying the load. Further description is given later in the experimental procedure section.

1.6 Applications

Due to a porosity of 70-90%, closed cell aluminum foams are very lightweight in nature. They can be used in various practical applications such as sandwich panels, crash and impact loadings, automotive frame structures and vibration reduction. Figures 1.4 illustrates the different applications of these foams in various industries. Because of their low cost, aluminum foams have become a desirable replacement to the existing applications of solid aluminum metal [27-31].

Aluminum foams are considered to be an excellent replacement for the glass-fiber reinforced plastic (GFRP) that are used in high speed trains (Figure 1.5) because both of these materials have the same stiffness but aluminum foams has an advantage because they are 20% lighter in weight and has better thermal stability in comparison [32,33]. Another major application of these foams is noise absorption. They have also been used in Japan under various expressways (Figure 1.6) [34].

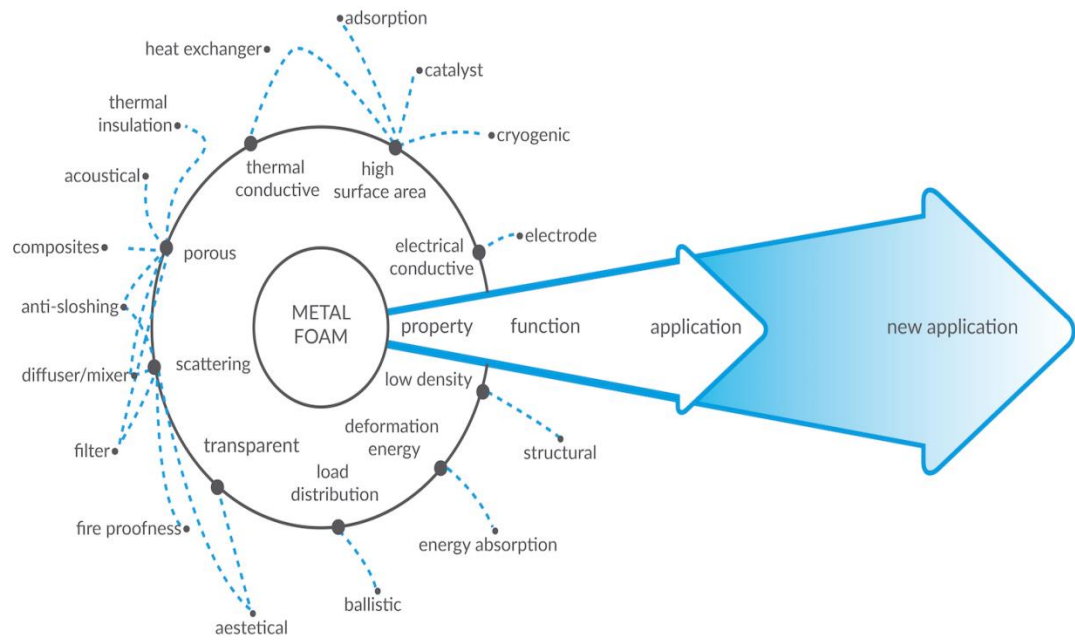


Figure 1.4 Applications of aluminum foams in various industries

Aluminum foams can be used as a core in sandwich structures (Figure 1.7) to improve their impact properties. There is still a huge scope of improvement in the mechanical properties of these foams, upon which aluminum foams could be used for a vast multitude of applications such as in the aerospace industry, they can be seen as a replacement for the much expensive honeycombs. Also, they might be used in car body structure (Figure 1.8) [35].

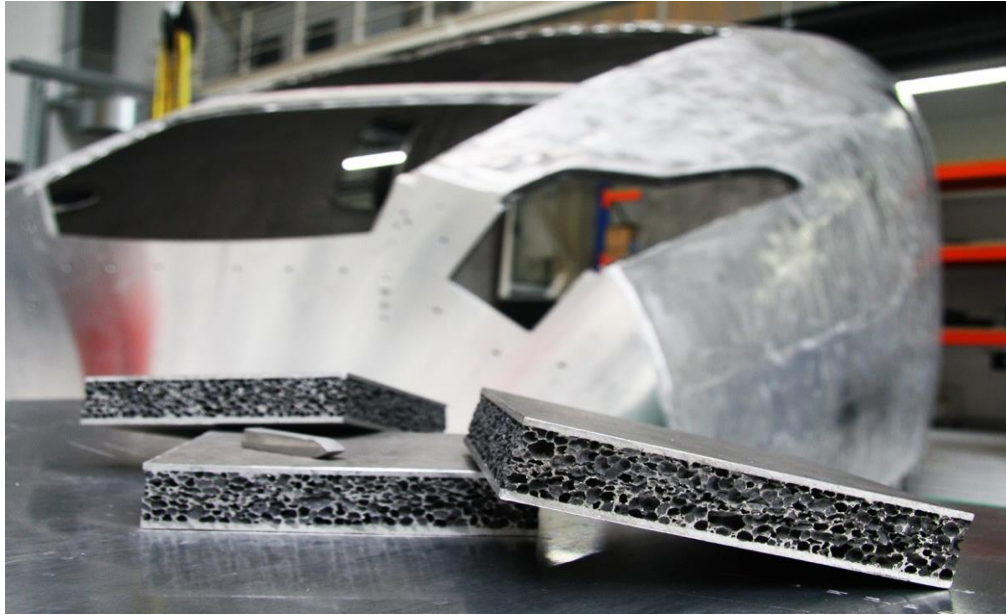


Figure 1.5 Application of Al-foams in high speed trains as a replacement of GFRP



Figure 1.6 Application of Al-foams in high speed trains as a replacement of GFRP

Figure 1.9 shows the application of aluminum foam used in a vacuum elevator tool to lift glass panels. Using aluminum foams for various parts helped in reducing the overall weight of the structure from 82 to 32 kg [36].



Figure 1.7 Application of Al-foams in high speed trains as a replacement of GFRP

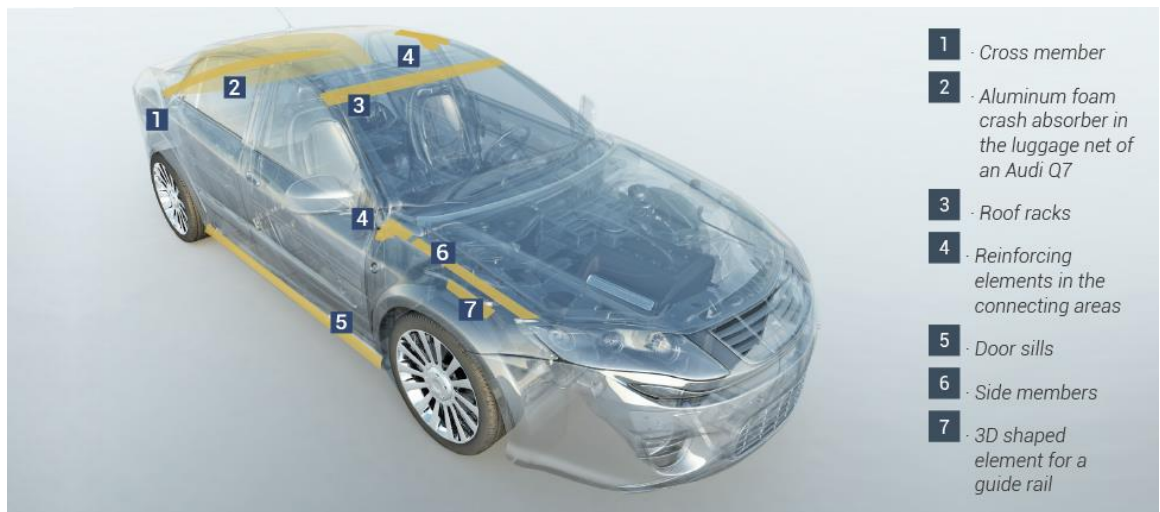


Figure 1.8 Aluminum foam used in car body structures



Figure 1.9 Vacuum lifting tool made of Al-foam

Another major application of aluminum foams in automobile industry is due to its property of high energy absorption. It is used in crash box (Figure 1.10) in the frontal bumper of cars since it can absorb more energy and lessen the damage on the car at the time of crash [37].

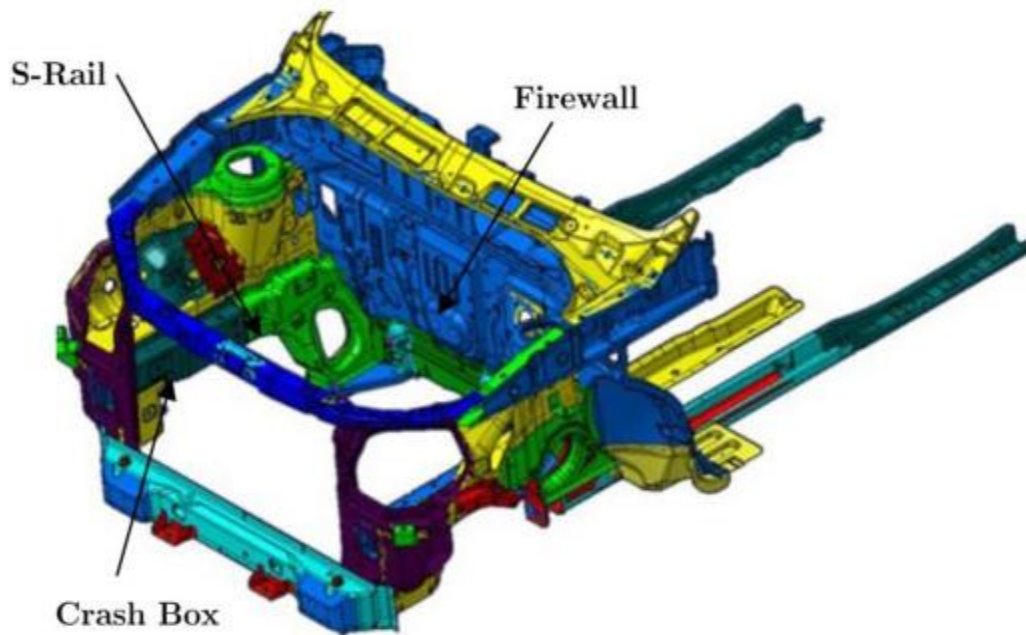


Figure 1.10 Al-foam used in crash box

1.7 Objective of this work

Aim of this research is to study the mechanical behavior of closed cell aluminum foams reinforced with graphene under various loading conditions. It is a lightweight material and has unique mechanical properties which need further investigation in order to have a better understanding of these properties.

The present study consists of examining several properties such as peak stress, plateau stress and energy absorption. Closed cell aluminum foam reinforced with graphene was produced by melt route. Further research of the material properties was done as a function of high temperature. A summary of objectives in this research is as follows:

The foam compositions studied had a graphene concentration of 0.2 wt.%, 0.4 wt. %, 0.5 wt.% and 0.62 wt.%. The strain rates achieved were in the range of 1000 s^{-1} – 2200 s^{-1} . The temperatures at which the mechanical behaviour of the foam was studied are room temperature (298 K) and high temperatures (473 °K and 623 °K)

1.8 Layout of this thesis

The present research has been organized into the following parts:

- Chapter 1 includes introduction, literature review and objective of the present work.
- Chapter 2 includes the experimental procedure, equipment and formulas used and testing methods at room and high temperature.
- Chapter 3 addresses the mechanical behavior of closed cell aluminum foams reinforced with graphene under dynamic loadings at room temperature.
- Chapter 4 presents with the effects of high temperature on the mechanical properties of the foams.
- Chapter 5 presents conclusions and future work.

CHAPTER TWO: EXPERIMENTAL METHODS

2.1 Split Hopkinson Pressure Bar (SHPB) theory

Split Hopkinson Pressure Bar is based on the theory of one dimensional elastic wave propagation [40]. Figure 2.1 presents the schematic description of working principle of SHPB. Subscripts I, T and R denote incident, transmitted and reflected pulses respectively and subscripts 1 and 2 represents the interface between incident bar and specimen and specimen and transmitted bar respectively [38].

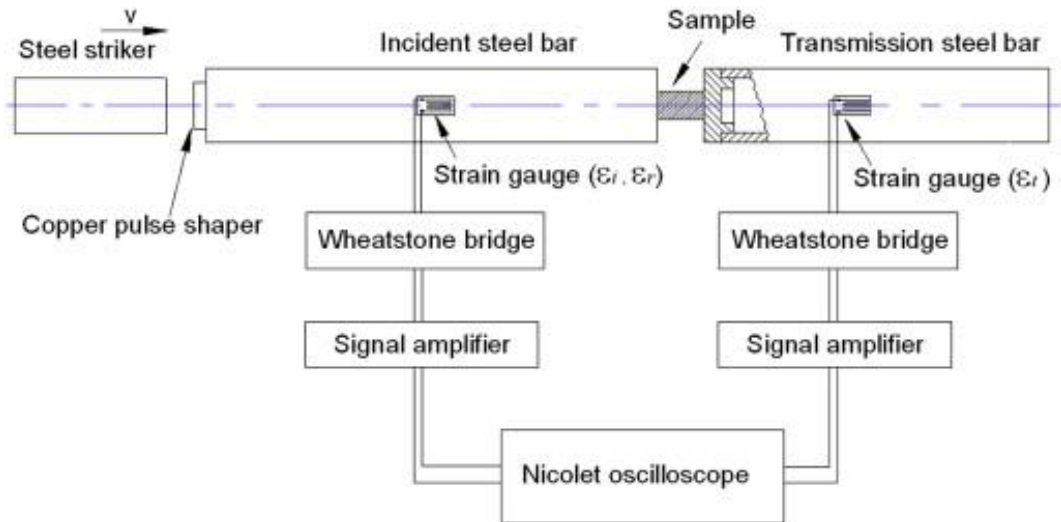


Figure 2.1 Schematic description of SHPB

1-D elastic wave propagation equation is given as following [39, 40]:

$$\frac{\partial^2 u}{\partial x^2} = \frac{1}{C_{OB}^2} \frac{\partial^2 u}{\partial t^2} \quad (2.1)$$

Where, C_{OB} is the sound velocity of the bar.

The solution of equation (2.1) by using D' Alembert's method gives us the incident bar and transmitted bar solution and is given by the following equations respectively:

$$u_1 = f(x - C_{OB}t) + g(x + C_{OB}t) = u_I + u_R \quad (2.2)$$

$$u_2 = h(x + C_{OB}t) \quad (2.3)$$

Where, f, g and h are arbitrary functions.

$$\text{Strain in incident bar:} \quad \varepsilon_1 = \frac{\partial u_1}{\partial x} = f' + g' = \varepsilon_I + \varepsilon_R \quad (2.4)$$

$$\text{Strain in transmitted bar:} \quad \varepsilon_2 = \frac{\partial u_2}{\partial x} = h' = \varepsilon_T \quad (2.5)$$

Particle velocity at the interface of incident and specimen:

$$\dot{u}_1 = \frac{\partial u_1}{\partial t} = -f' \cdot C_{OB} + g' \cdot C_{OB} = C_{OB}(g' - f') = C_{OB}(\varepsilon_R - \varepsilon_I) \quad (2.6)$$

Particle velocity at the interface of specimen and transmitted bar:

$$\dot{u}_2 = \frac{\partial u_2}{\partial t} = -C_{OB} \cdot \varepsilon_T \quad (2.7)$$

When the elastic stress wave propagation is neglected, the average strain rate in the specimen is given as:

$$\dot{\varepsilon}_S = \frac{(u_1 - u_2)}{H_S} = \frac{C_{OB}}{H_S} (-\varepsilon_I + \varepsilon_R + \varepsilon_T) \quad (2.8)$$

The forces in incident bar and transmitted bars are:

$$F_1 = A_B E_B (\varepsilon_I + \varepsilon_R) \quad (2.9)$$

$$F_2 = A_B E_B \varepsilon_T \quad (2.10)$$

Where, H_s is the instantaneous length of the specimen

A_B is the cross section area of the SHPB bars

E_B is the elastic Young's modulus of the SHPB bars

In order to achieve uniaxial stress equilibrium, the forces F_1 and F_2 have to be the same.

$$(F_1 = F_2)$$
$$\varepsilon_L + \varepsilon_R = \varepsilon_T \quad (2.11)$$

Substituting equation (2.11) into (2.8) we get average strain rate in the specimen:

$$\dot{\varepsilon}_s = \frac{2C_{OB}\varepsilon_R}{H_s} \quad (2.12)$$

Average true stress in the specimen is given by the equation (2.13)

$$\sigma(t) = \frac{F_2}{A_s} = \frac{A_B E_B \varepsilon_T}{A_s} \quad (2.13)$$

Where A_s is the instantaneous cross section area of the specimen.

The expressions for average engineering stress and engineering strain of the specimen is given by the following equations:

$$\sigma_s(t) = \left(\frac{A_B E_B}{A_{s0}} \right) \varepsilon_T(t) \quad (2.14)$$

$$\varepsilon_s(t) = \left(\frac{2C_{OB}}{H_{s0}} \right) \int^t \varepsilon_R(t) dt \quad (2.15)$$

2.2 Assumptions of a valid SHPB test

Gama [39] and Chen [41] reviewed the assumptions needed for SHPB test. SHPB bar system must have explicit characteristics for the generation of 1-D elastic wave propagation during the test for the solutions of equations (2.14) and (2.15) to follow the principle of 1-D elastic wave propagation. For this a thin, long rod which has linear elastic, isotropic, uniform and homogenous characteristic is used as the incident and transmitted bar. Equation (2.8) is valid only when C_{OB} is same in equations (2.2) and (2.5). Similarly, when A_B and E_B are same in equations (2.9) and (2.10) then only equation (2.11) can be formulated.

We can infer from equations (2.12) and (2.15) that applied strain rate; $\dot{\epsilon}_S$ has a substantial influence on the mechanical behavior of the materials that are sensitive to strain rate. Thus, having stress equilibrium and a constant strain rate in the specimen is essential for validating a test on SHPB apart from generating 1-D stress wave propagation.

2.3 Experimental Set up

Dynamic compression testing for various materials can be performed using SHPB apparatus. Materials like metals, polymeric composites and ceramics can be tested under large strain rates up to several thousand per second. Dynamic compressive tests are more commonly used when compared to dynamic tension and torsion tests due to its simplicity

in testing techniques and sample designs. Figure 2.2 shows the schematics of the in house SHPB system used in this study.

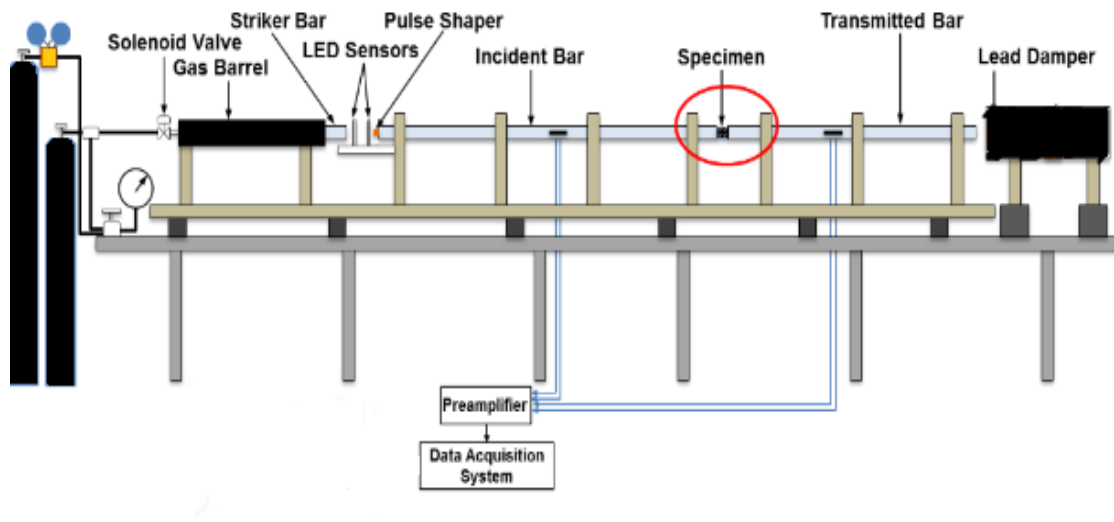


Figure 2.2 Schematic diagram of SHPB system

When the gas gun is launched, the striker bar present in the gas barrel hits the incident bar and an elastic compression wave (known as incident wave) travels in the incident bar. Once this incident wave hits the specimen which has been sandwiched between the incident and transmitted bars, it splits in to two different waves namely, reflected wave which is reflected back in the incident bar and a transmitted wave which travels through the transmitted bar. These waves are collected by strain gages that are mounted on the incident and transmitted bars respectively [42].

The SHPB apparatus has four main parts namely:

- Gas launcher assembly
- Pressure bar assembly
- Data acquisition system
- Supporting and damping system

2.3.1 Gas launcher assembly

It is a crucial part of the SHPB system as the entire apparatus works with nitrogen gas. It has the following main components: Solenoid valve, pressure tanks, pressure regulator and gun barrel. Figure 2.3 shows the gas launcher assembly in the lab.

Two pressure tanks are joined through a sealed pipe and pressure regulator. Black tank is a reservoir which stores compressed nitrogen gas which then subsequently used to fill the blue tank at the desired pressure which can be regulated by using a pressure regulator. Solenoid valve opens and releases the compressed nitrogen gas through the gas barrel for a preset time by the user. It is controlled by a computerized system.

Two pressure regulators are used in this system. The first pressure regulator shows the current pressure in the tank and the second regulators shows the delivery pressure to the solenoid valve. Gun barrel is a hollow cylindrical tube made of steel and is screwed onto

flanges at the ends. It is 120 mm long having 32 mm external diameter and 20 mm internal diameter.



Figure 2.3 Gas launch assembly of in-house SHPB apparatus

2.3.2 Pressure bar assembly

A pressure bar assembly consists of striker bar (Figure 2.4), incident bar (Figure 2.5) and transmitted bar (Figure 2.6). All three bars are of same dimensions and materials as they are the two most important factors. The pressure bar material should have low wave attenuation on both radial and longitudinal dimensions (small Poisson's ratio) and high sensitivity to signal-to-noise. Besides, signal loss is almost zero. High strength structural material like steel is traditionally used for SHPB bar material; however, the SHPB test will not guarantee accuracy. The reason is due to significant strength differences between the bar and specimen materials. Wave impedance ($\rho \cdot C_0$) of low strength materials such as aluminum foam is much lower than that of the Al pressure bar; therefore, most of the

incident pulse is reflected backward into the incident bar and only a small portion of loading is transmitted through specimen to transmitted bar. As a result, transmitted pulses become very weak even with the use of high strain-gage gain, making it impossible to get the precise and complete transmitted pulses. Even when such small transmitted signals are collected precisely and completely, it is not easy to check stress equilibrium with these signals. In dynamic equilibrium checking, a comparison is made between transmitted signal and the difference of incident and reflected signals. Obviously, the comparison of a very small signals with two large-amplitude ones must be inaccurate [43].

In the SHPB system used for the present study, aluminum 7075-T6 was taken to be the pressure bar material whose mechanical properties are shown in Table 2.1. These bars should be straight and be aligned on the same axis. Function of the striker bar is to change the pulse duration in the incident pulse or incident propagating wavelength. The amplitude of the pulse is directly proportional to the length of the striker bar as well as the impact velocity which can be varied with pressure.



Figure 2.4 Aluminum striker bar with 457.2 mm in length and 12.7 mm in diameter

Table 2.1 Properties of SHPB components

Part	Material	Length (mm)	Diameter (mm)	Young's Modulus (GPa)	Density (Kg/mm³)
Gas Barrel	Steel	1200	32(outer) and 20 (inner)	210	~7800
Striker Bar	Aluminum	457.2	12.7	71.7	~2800
Incident Bar	Aluminum	1820	12.7	71.7	~2800
Transmitted Bar	Aluminum	1370	12.7	71.7	~2800

The striker bar comes into contact with the incident bar directly whereas the transmitted bar makes an indirect contact. When the striker bar makes contact with the incident bar a compressive incident wave is propagated across the bar which meets the specimen that is sandwiched between the two bars. Part of the wave gets reflected at the incident-specimen interface whereas the remaining wave gets transmitted to the second bar. The two bars are mounted with strain gages which give the magnitude and shape of the incident, transmitted and reflected pulses. Dimensions of pressure bars including length (l) and diameter (d), are chosen to meet a criteria of 1-D wave propagation for a given pulse length. For experimental measurements on most engineering materials, this propagation requires about 10 bar diameters. Also, the incident bar length should be at least twice as long as the striker bar's to avoid overlapping between the incident and reflected pulses [44].

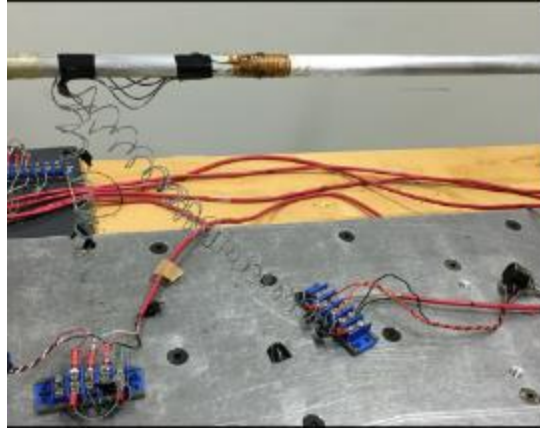


Figure 2.5 Incident bar in the SHPB apparatus



Figure 2.6 Transmitted bar in the SHPB apparatus

Figure 2.6 shows a momentum trap for the transmitted bar to stop it after being struck by the incident bar. Lead is used as a softer material to prevent the damage to the back end of the transmitted bar.



Figure 2.6 Damping system

2.3.3 Data acquisition system

Data acquisition system consists of strain gages, LED sensors, LabVIEW and preamplifier. A strain gage is a device whose resistance varies proportionally to the change of strain. It is the most common method to measure strain due to its convenient size and easy installation. It is made of metallic strip that are arranged in a grid pattern. In order to reduce the errors in measurements, following things need to be taken care of –

- a) Use of good adhesive between carrier and aluminum bars
- b) Direction of strain gage must be parallel to neutral axis of SHPB bar
- c) Proper calibration must be done before actual testing

A quarter bridge circuit was used in this system. It has four arms (resistance) as shown in Figure 2.7. R_1 and R_3 are set up to be equal and R_2 is set to equal the strain gage resistance. Therefore when no force is applied, the circuit is symmetric and should read

zero point. When a compressive pulse travels through the bar, the metallic strips deform elastically and the deformation is measured in millivolt [44].

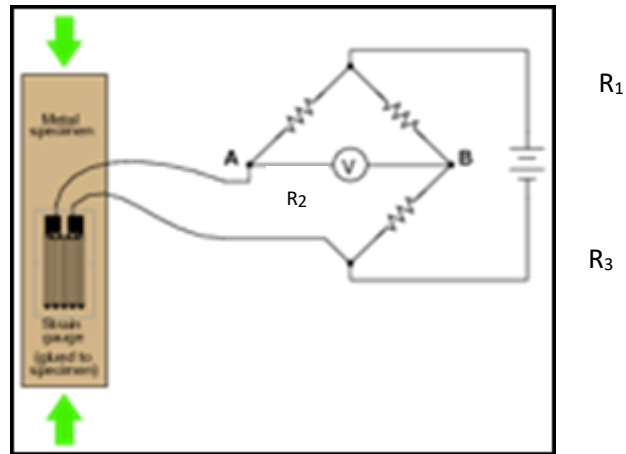


Figure 2.7 A quarter bridge strain gage circuit

Equations use for the strain gage voltage as a function of strain is:

$$\frac{V_0}{V_{EX}} = -\frac{GF \cdot \epsilon}{4} \left(\frac{1}{1 + GF \cdot \frac{\epsilon}{2}} \right) \quad (2.16)$$

$$GF = \frac{\Delta R/R}{\Delta L/L} = \frac{\Delta R/R}{\epsilon} \quad (2.17)$$

Where,

V_0 is the strain gage output voltage

V_{EX} is excitation voltage of 10 mv

ϵ is the recorded signal from strain gage in mv

GF is the strain gage factor of 2.7

Figure 2.8 a and b depicts the measured data from strain gages mounted on incident and transmitted bar respectively. The incident and reflected pulse are given by the first downward and upward pulse as shown in Figure 2.8a. Whereas, the transmitted pulse is given by the first downward pulse in Figure 2.8b.

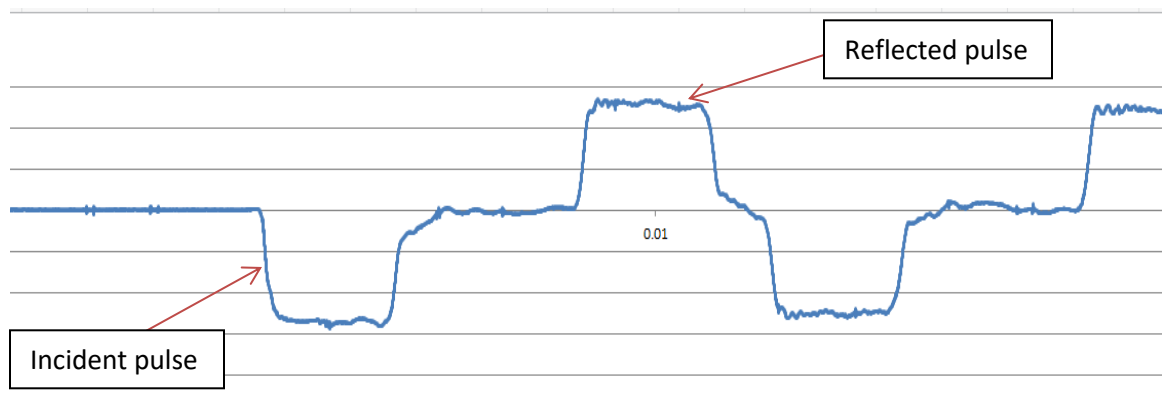


Figure 2.8 A measured incident and reflected pulse

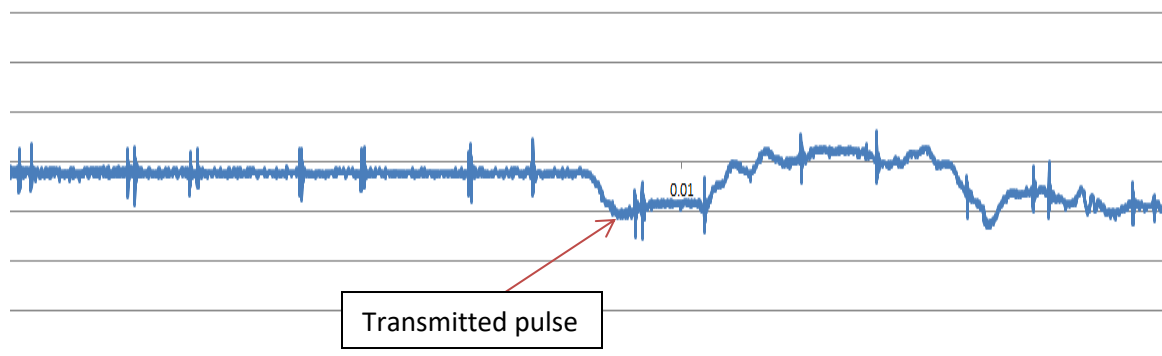


Figure 2.8 A measured transmitted pulse

A Tektronix ADA400A differential Preamplifier was used with upper bandwidth filters of 100100Hz, 3kHz, 100kHz and Full (>1MHz), as shown in Figure 2.9. It was used to enable the strain gages to measure the data during the tests.

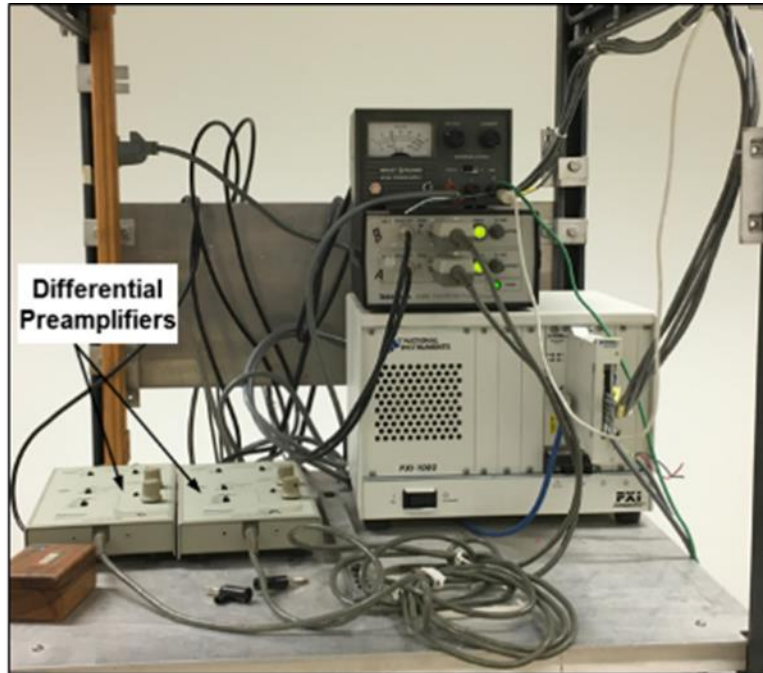


Figure 2.9 Differential preamplifiers and PXI system

LabVIEW was used to test and measure data from strain gages. Figure 2.10 shows the interface of LabVIEW window which includes incident, reflected, transmitted and LED light pulse. The interface consists of SHPB experiment constants like sample rate, sample per channel and solenoid valve time. Figure 2.11 shows the expanded view of the constants.

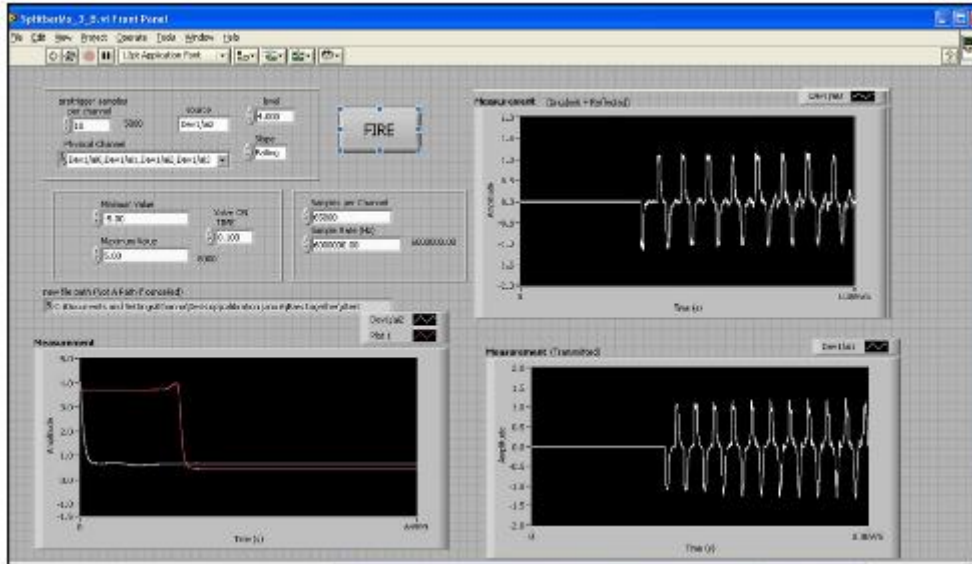


Figure 2.10 LabVIEW interface

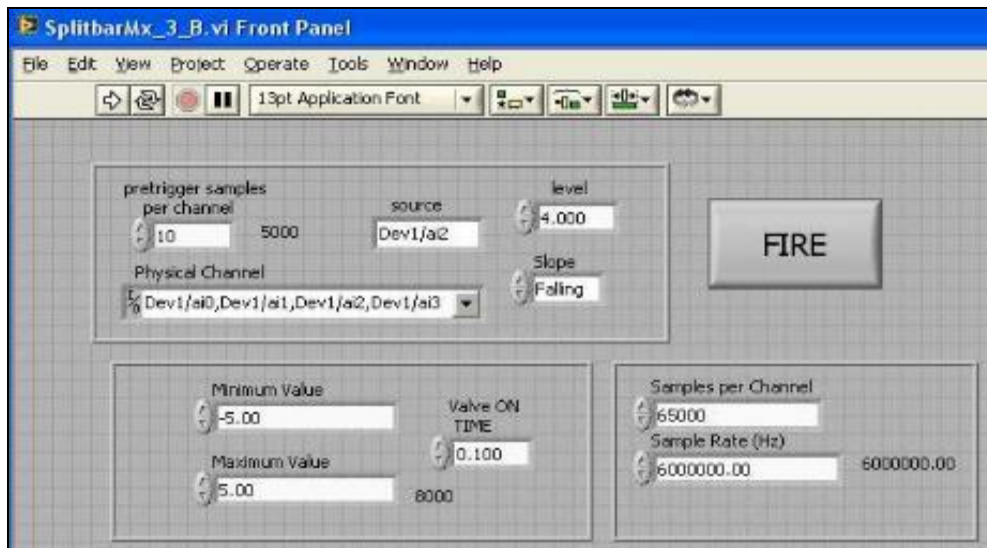


Figure 2.11 Experimental constants in LabVIEW interface

2.4 Working principle

A desired pressure is set on the gas tank based on the strain rate that is required for the test using pressure regulators. The striker bar is pushed to the back of the gas barrel and specimen is kept between the incident and the transmitted bar. A very thin layer of molybdenum grease was applied to reduce friction between specimen and the bars. Pulse shaper is placed on the front of the incident bar as shown in Figure 2.12. Next, the striker bar is launched through the gas barrel and a compressive wave is generated once it impacts the incident bar. This compressive wave travels across the incident bar and at the interface of the back end of the incident bar and specimen, part of the wave is reflected as a tensile wave and the remaining part is transmitted through the specimen as a compressive wave and into the transmitted bar.

The distance between two LED lights is 63.82 mm which is already known therefore, the velocity of the striker bar is calculated by determining the time it takes for the striker bar to pass the two LED lights. Figure 2.13 shows the in-house SHPB system.

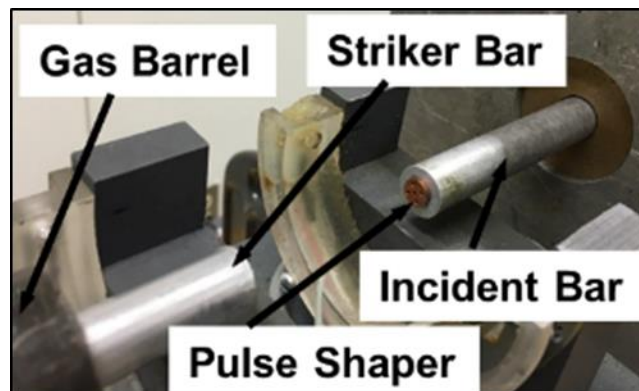


Figure 2.12 Pulse shaper, striker bar and incident bar



Figure 2.13 An overview of in-house SHPB system

2.5 Calibration

There are a lot of factors like bars machining, strain gage insulation effect and assembly effect that affect the accuracy of the measured signals. Therefore, calibration is an essential step to be performed before any tests. Machining and assembly factors vary the accuracy of the measured data as the bars may not have the exact cross section over the entire length of the bar. It should also be done whenever a strain gage is replaced on the pressure bar and when the bars are changed. The erroneousness on the SHPB system is corrected using the calibration factors such as strain correction factor (K_ϵ) for incident $K_\epsilon(I)$ and transmitted $K_\epsilon(T)$ bars and stress correction factor (K_σ).

The equations used for calibration of SHPB are:

$$K_{\varepsilon} = \frac{\varepsilon_B^{Calculated}}{\varepsilon_B^{Measured}} \quad (2.18)$$

$$\varepsilon_B^{Calculated} = \frac{\sigma_B}{E_B} \quad (2.19)$$

Where, E_B is the young's modulus of the bar and σ_B is stress in bar

$$\sigma_B = \rho_B \cdot C_{OB} \cdot \dot{u} \quad (2.20)$$

Where, ρ_B is density of the bar, C_{OB} is velocity of sound in the bar and \dot{u} is particle velocity in the stress pulse

$$C_{OB}^2 = \frac{E_B}{\rho_B} \quad (2.21)$$

$$\dot{u} = \frac{V_{SB}}{2} \quad (2.22)$$

Therefore, $\varepsilon_B^{Calculated}$:

$$\varepsilon_B^{Calculated} = \frac{\sigma_B}{E_B} = \frac{\rho_B \cdot C_{OB} \cdot \dot{u}}{E_B} = \frac{\rho_B \cdot C_{OB} \cdot V_{SB}}{2E_B} = \frac{C_{OB} \cdot V_{SB}}{2C_{OB}^2} = \frac{V_{SB}}{2C_{OB}} \quad (2.23)$$

$$V_{SB} = \frac{L_{SB}}{t_{SB}} \quad (2.24)$$

Where,

L_{SB} is the length between first and second LED sensors of 63.818 mm. t_{SB} is the time it takes the striker bar to travel between first and second LED sensors.

$\varepsilon_B^{Measured}$ is calculated via the recorded strain gage signal in millivolt and is converted to strain using a MATLAB code using equations (2.25) and (2.26).

$$\frac{V_o}{V_{Ex}} = \frac{-GF \cdot \varepsilon_B^{Measured}}{4} \left(\frac{1}{1 + GF \frac{\varepsilon_B^{Measured}}{2}} \right) \quad (2.25)$$

$$\varepsilon_B^{Measured} = \frac{-4\varepsilon_{mv}}{G \cdot GF \left(V_{Ex} + \frac{2\varepsilon_{mv}}{G} \right)} \quad (2.26)$$

Where, V_o is the strain-gage output voltage $V_o = \frac{\varepsilon_{mv}}{G}$, ε_{mv} is the recorded signal from strain gage in mv, V_{Ex} is the excitation voltage of 10 mv, GF is the strain-gage factor of 2.7, and G is gain factor of 100.

The corrected strain signals for incident and transmitted bars are given in equations (2.27) and (2.28), respectively.

$$\varepsilon_I^{Corrected} = K_\varepsilon(I) \cdot \varepsilon_I^{Measured} \quad (2.27)$$

$$\varepsilon_T^{Corrected} = K_\varepsilon(T) \cdot \varepsilon_T^{Measured} \quad (2.28)$$

Also, K_σ is then given in equation (2.29).

$$K_\sigma = \frac{\varepsilon_B^{Incident}}{\varepsilon_B^{Transmitted}} \quad (2.29)$$

$$\sigma_S^{Calculated} = \left(\frac{A_B \cdot E_B}{A_{SO}} \right) \cdot \varepsilon_T^{Corrected} \quad (2.30)$$

$$\sigma_S^{Corrected} = K_\sigma \cdot \sigma_S^{Calculated} \quad (2.31)$$

Where, A_B and E_B are the cross-sectional area and elastic Young's modulus of SHPB bars. A_{SO} is the original area cross-sectional area of the specimen.

Table 2.2 shows the strain corrections factors for incident and transmitted bars which have been calculated after the calibration whereas, Table 2.3 shows the stress correction factors.

Table 2.2 Strain correction factors for incident and transmitted bars

	Pressure (psi)	Incident				Transmitted			
		13	17.5	28	40	13	17.5	28	40
Time Travel	W/O I	0.00810325	0.006515	0.0045802	0.003723667	0.0070233	0.006499	0.0046113	0.003676167
	W/O II	0.00833925	0.0065115	0.0046188	0.0036825	0.0081648	0.006864	0.0046497	0.003645667
	W I	0.007859918	0.006084	0.0045827	0.003726	0.0073548	0.0063885	0.0045845	0.0036755
	W II	0.00826375	0.0066537	0.0044155	0.003728167	0.0070255	0.0060483	0.0043982	0.0037055
Speed (mm/s)	W/O I	7875.698022	9795.6639	13933.718	17138.685	9086.7185	9819.78	13839.544	17360.135
	W/O II	7652.8165	9800.9291	13817.071	17330.278	7816.3753	9297.6034	13725.446	17505.372
	W I	8119.518748	10489.604	13926.117	17127.952	8677.2154	9989.6298	13920.547	17363.284
	W II	7722.734836	9591.516	14453.346	17117.998	9083.873	10551.46	14510.307	17222.709
MEASURED STRAIN [MATLAB]	W/O I	8.36E-04	0.0011571	0.0016682	0.0020092	0.001039	0.0013181	0.0017299	0.0021656
	W/O II	8.17E-04	0.0011856	0.0016587	0.0020802	8.92E-04	0.001247	0.0017345	0.0021988
	W I	8.31E-04	0.0011666	0.0015641	0.0018765	9.40E-04	0.0012234	0.0016682	0.0019714
	W II	7.51E-04	0.0010862	0.0015877	0.0018955	0.001039	0.001266	0.0016587	0.0020045
Calculated strain m/m	W/O I	0.000779618	0.0009697	0.0013793	0.0016966	0.0008995	0.0009721	0.00137	0.0017185
	W/O II	0.000757555	0.0009702	0.0013678	0.0017155	0.0007737	0.0009204	0.0013587	0.0017329
	W I	0.000803754	0.0010384	0.0013786	0.0016955	0.000859	0.0009889	0.001378	0.0017188
	W II	0.000764476	0.0009495	0.0014307	0.0016945	0.0008992	0.0010445	0.0014364	0.0017049
STRAIN CORRECTION FACTOR	W/O I	0.932894	0.8379985	0.8268264	0.8444002	0.8657413	0.7374592	0.7919627	0.7935317
	W/O II	0.927327915	0.8183119	0.8246011	0.8246874	0.8670215	0.7380587	0.7833259	0.7880912
	W I	0.96715155	0.8900629	0.8813846	0.9035504	0.914121	0.8083132	0.8260448	0.871885
	W II	1.018312946	0.8740826	0.9011262	0.8939682	0.8654702	0.8250304	0.8659733	0.8505113

Table 2.3 Stress correction factors

	Pressure (psi)	Incident Strain from Matlab				Transmitted Strain from Matlab			
		13	17.5	28	40	13	17.5	28	40
MATLAB	W/O I	7.18E-04	0.0012046	0.0016682	0.0021466	7.88E-04	0.0015119	0.0021181	0.0026111
	W/O II	7.46E-04	0.0013418	0.0017392	0.0020944	9.44E-04	0.001635	0.0021229	0.0025495
	W I	6.66E-04	0.0011997	0.0015594	0.0018482	6.70E-04	0.0012943	0.0016682	0.0019477
	W II	7.88E-04	0.001181	0.0015451	0.0018103	8.07E-04	0.0012424	0.0015831	0.0018718
STRESS CORRECTION FACTOR	W/O I	0.910161431	0.7967259	0.7876014	0.8221049				
	W/O II	0.789721059	0.8206344	0.8192337	0.8214848				
	W I	0.992784188	0.9269538	0.9347986	0.9489033				
	W II	0.976507791	0.9505704	0.9759979	0.96715				

Where, W/O I and W/O II are calibration tests performed without pulse shaper and W I and W II are calibration tests performed with pulse shapers.

Incident strain, reflected strain and transmitted strain are determined by using the following equations:

$$\epsilon_I = \frac{4\epsilon_{I \text{ Recorded in mV}}}{G * GF \left(V_{Ex} + \frac{2\epsilon_{I \text{ Recorded in mV}}}{G} \right)} \quad (2.32)$$

$$\epsilon_R = \frac{4\epsilon_{R \text{ Recorded in mV}}}{G * GF \left(V_{Ex} + \frac{2\epsilon_{R \text{ Recorded in mV}}}{G} \right)} \quad (2.33)$$

$$\epsilon_T = \frac{4\epsilon_{T \text{ Recorded in mV}}}{G * GF \left(V_{Ex} + \frac{2\epsilon_{T \text{ Recorded in mV}}}{G} \right)} \quad (2.34)$$

2.6 Graphene reinforced Aluminum foam fabrication

The graphene reinforced aluminum foams were fabricated at CSIR-AMPRI, India and the specimens were made at University of Missouri, Columbia. Liquid melt route process was used for the fabrication of the foam. The steps involved were as follows:

1. The Al alloy selected as the base material was AA5083 combined with SiC particle of 10 wt. %. Graphene was used as a thickening agent. 1 wt. % Titanium Hydride (TiH_2) was used a foaming agent.
2. Raw material was placed in the mold and melted at 800°C .
3. The melt was stirred using a mechanical stirrer at a speed of 700 rpm.
4. Melt was then mixed with SiC particles and graphene.
5. Once the particles were mixed properly, then the foaming agent was added in the melt.
6. Once the foaming was over, the mold containing is rapidly cooled with air jet to freeze the foam.

The specimens were prepared using a low speed diamond saw wheel (Figure 2.14). The dimensions of specimens is selected based on the works of Mukaii *et al.* [13], Hamada *et al.* [16] and Raj *et al.* [19] which was ~80% of the SHPB bar diameter. The properties of closed cell aluminum foams depend on the relative density (density of foam/density of solid aluminum). Density of foam was computed by measuring the dimensions using a digital caliper and the specimens were weighed using a digital balance. Figure 2.15 shows the example of the specimen used in SHPB testing.



Figure 2.14 Low speed diamond wheel saw



Figure 2.15 Specimen used in SHPB testing

2.7 Pulse shaping technique

A 145 Tellurium copper pulse shaper disk has been used in the present work as it can undergo large strain without fracturing. A pulse shaper as discussed above is placed at the front end of the incident bar. The pulse shaper diameter D_{PS} to bar diameter D_B ratio is selected to be equal to 0.5 [44]. There are multiple advantages of using a pulse shaper such as:

1. It minimizes the stress wave dispersion
2. It enables stress equilibrium
3. It increases accuracy of measuring Young's modulus from stress strain curve

According to literature, it was suggested that pulse shaper should be of the same materials as that of the specimen [45] however, Vecchio *et al.* [46] showed that it's not necessary to use the same material as that of the specimen. Most common materials used for pulse shaper are plexiglass, stainless steel, brass or copper.

A thin film of molybdenum grease was used to hold the pulse shaper at the front end of the incident bar. Table 2.4 presents the properties of the copper pulse shaper. The pulse shaper used in the present study has five holes of 1 mm each that have been drilled symmetrically as shown in Figure 2.16 [44].

Table 2.4 Properties of Tellurium copper pulse shaper

Chemical Composition % by weight			Physical Properties		Mechanical Properties			
Copper %	Phosphorous %	Tellurium %	Density g/cm ³	Elastic Modulus (GPa)	Rockwell Hardness B Scales	Tensile strength (MPa)	Yield strength (MPa)	Elongation (% in 2 inch)
99.7	0.008	0.55	8.94	117.211	48	330.95	303.369	20



Figure 2.16 A five hole pulse shaper

During the initial tests, it was found that without the use of pulse shaper stress equilibrium was not achieved as seen in Figure 2.17. But with the use of a five holed pulse shaper good stress equilibrium was observed (Figure 2.18). Diameter of the pulse shaper used was 6.35 mm with each hole of 1 mm each. This enabled enough material to be left between holes for the wave to travel through. Use of pulse shaper also enables to achieve a constant strain rate which was not attained when there was no pulse shaper used as seen in Figure 2.19. Use of pulse shaper led to a constant strain rate in the closed cell foam specimen (Figure 2.20).

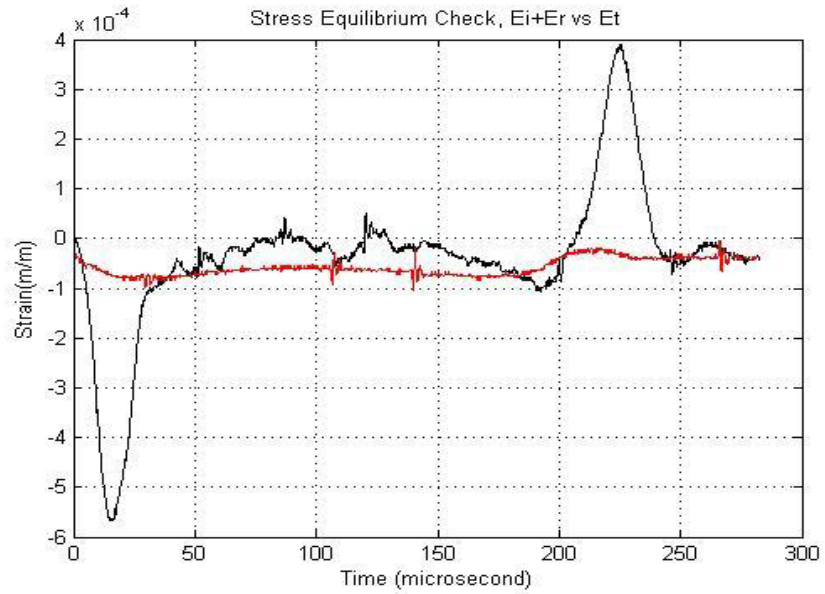


Figure 2.17 Stress equilibrium without pulse shaper

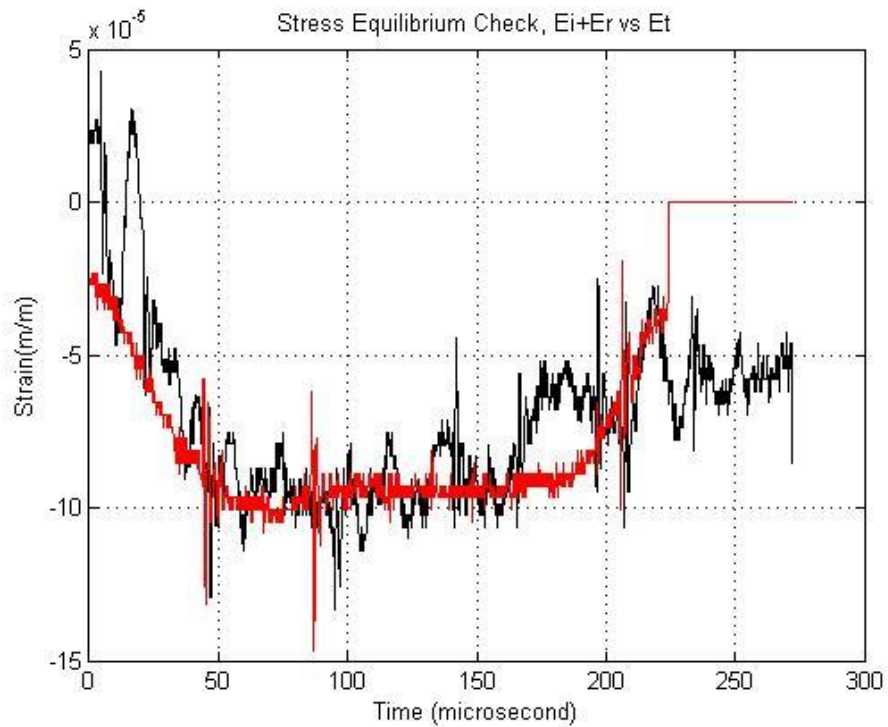


Figure 2.18 Stress equilibrium with the use of five holed pulse shaper

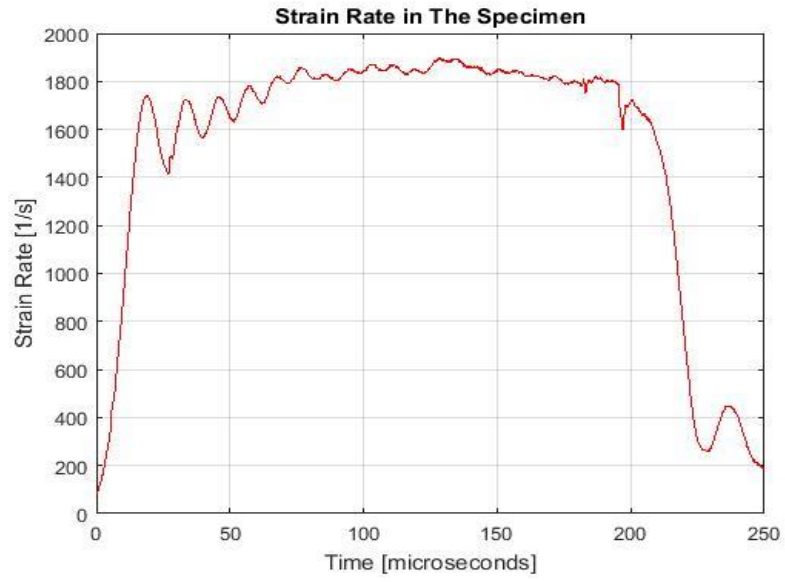


Figure 2.19 Strain rate without pulse shaper

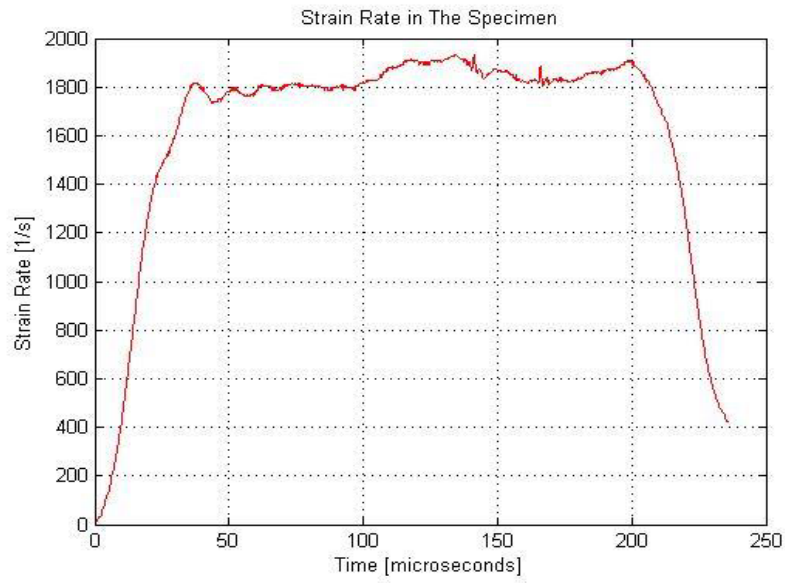


Figure 2.20 Strain rate with pulse shaper

2.8 Effect of strain rate at high temperature

Dynamic compression tests were performed at high temperatures of 200 °C (473 K) and 350 °C.(623 K) Specimen was heated using an infrared heating element before conducting the high strain rate test. The specimen was kept on a stand and aligned with the axis of the bars as shown in Figure 2.21. A thermocouple was inserted inside the specimen to keep track of the temperature. When the specimen reaches the desired temperature, the incident and transmitted bars are brought in contact with the specimen and the stand is lowered and striker is launched. Heating is continued during the entire process and a thin layer of super enhanced graphite was used to reduce friction between the bars and the specimen [47].

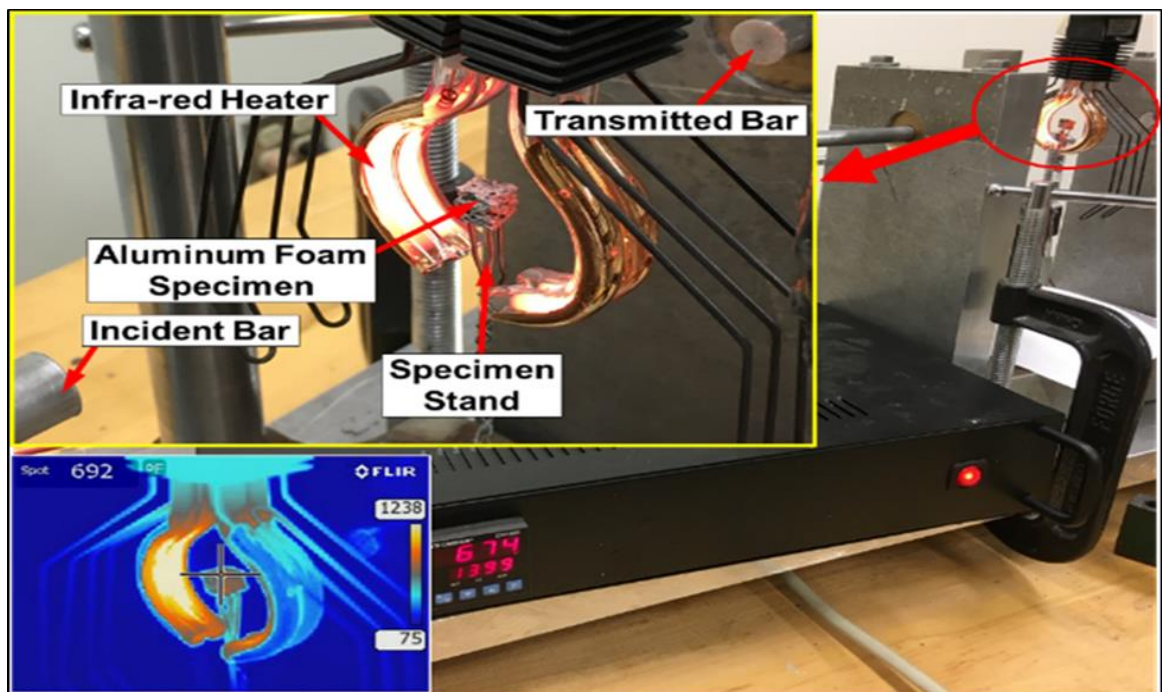


Figure 2.21 Setup of high temperature in SHPB system

2.9 Data analysis

The data recorded by the strain gages are analyzed in Excel so as to select the required data which is the input for the SHPB MATLAB file. The MATLAB file will subsequently give the output like the strain rate time, stress time, stress-strain curve and stress equilibrium check.

Figure 2.22 shows a portion of the Excel file. Columns A and B presents the recorded data from the incident and transmitted strain gages respectively whereas, columns C and D present the data obtained from the first and second LED lights.

	A	B	C	D	E	F	G
1	t0	dt	y				
2	3.6E+09	3.6E+09	3.6E+09	3.6E+09			
3	0	0	0	0			
4	-0.0073	-0.0098	4.0015	4.1309			
5	-0.0073	-0.0098	3.9966	4.1284			
6	-0.0098	-0.0146	3.9917	4.1235			
7	-0.0073	-0.0098	3.9941	4.126			
8	-0.0073	-0.0122	3.9941	4.1284			
9	-0.0098	-0.0122	3.9917	4.126			
10	-0.0073	-0.0122	3.9868	4.1235			
11	-0.0122	-0.0171	3.9868	4.126			
12	-0.0098	-0.0122	3.9917	4.1309			
13	-0.0122	-0.0146	3.9844	4.126			
14	-0.0098	-0.0122	3.9819	4.1235			
15	-0.0098	-0.0122	3.9844	4.126			
16	-0.0098	-0.0122	3.9819	4.126			
17	-0.0098	-0.0122	3.9819	4.1284			
18	-0.0098	-0.0098	3.9795	4.126			
19	-0.0098	-0.0146	3.9771	4.126			
20	-0.0098	-0.0122	3.9771	4.126			
21	-0.0098	-0.0122	3.9771	4.1284			
22	-0.0098	-0.0098	3.9746	4.1284			
23	-0.0098	-0.0122	3.9746	4.126			
24	-0.0098	-0.0098	3.9722	4.126			
25	-0.0073	-0.0122	3.9722	4.1284			
26	-0.0073	-0.0122	3.9697	4.126			
27	-0.0073	-0.0098	3.9673	4.126			
28	-0.0098	-0.0122	3.9697	4.1284			
29	-0.0171	-0.0195	3.9697	4.1309			
30	-0.022	-0.0244	3.9697	4.1333			
31	-0.0244	-0.0293	3.9575	4.1211			

The figure shows an Excel spreadsheet with columns A through G. Red arrows point from text boxes to specific data points: 'Light 2' points to row 6, column D; 'Light 1' points to row 10, column D; 'Transmitted data' points to row 20, column D; and 'Incident data' points to row 24, column D. Row 17 is highlighted in yellow.

Figure 2.22 SHPB data in Excel before modifying

The next step is to delete the first two rows and add two columns of ascending order and time as shown in Figure 2.23. The incident and transmitted signals are plotted on separate graphs (Figure 2.24) and the first set of data is then selected by zooming in both the graphs. The first downward curve in the incident graph gives the incident data and the first upward curve in the incident graph gives the reflected data whereas, the first downward curve in transmitted graph gives the transmitted data.

B2 fx =A2/6000000

	A	B	C	D	E	F	G	H	I
1	Order	Time	t0	dt	y				
2	1	1.66667E-07	-0.0073	-0.0098	4.0015	4.1309			
3	2	3.33333E-07	-0.0073	-0.0098	3.9966	4.1284			
4	3	0.0000005	-0.0098	-0.0146	3.9917	4.1235			
5	4	6.66667E-07	-0.0073	-0.0098	3.9941	4.126			
6	5	8.33333E-07	-0.0073	-0.0122	3.9941	4.1284			
7	6	0.000001	-0.0098	-0.0122	3.9917	4.126			
8	7	1.16667E-06	-0.0073	-0.0122	3.9868	4.1235			
9	8	1.33333E-06	-0.0122	-0.0171	3.9868	4.126			
10	9	0.0000015	-0.0098	-0.0122	3.9917	4.1309			
11	10	1.66667E-06	-0.0122	-0.0146	3.9844	4.126			
12	11	1.83333E-06	-0.0098	-0.0122	3.9819	4.1235			
13	12	0.000002	-0.0098	-0.0122	3.9844	4.126			
14	13	2.16667E-06	-0.0098	-0.0122	3.9819	4.126			
15	14	2.33333E-06	-0.0098	-0.0122	3.9819	4.1284			
16	15	0.0000025	-0.0098	-0.0098	3.9795	4.126			
17	16	2.66667E-06	-0.0098	-0.0146	3.9771	4.126			
18	17	2.83333E-06	-0.0098	-0.0122	3.9771	4.126			
19	18	0.000003	-0.0098	-0.0122	3.9771	4.1284			
20	19	3.16667E-06	-0.0098	-0.0098	3.9746	4.1284			
21	20	3.33333E-06	-0.0098	-0.0122	3.9746	4.126			
22	21	0.0000035	-0.0098	-0.0098	3.9722	4.126			
23	22	3.66667E-06	-0.0073	-0.0122	3.9722	4.1284			
24	23	3.83333E-06	-0.0073	-0.0122	3.9697	4.126			
25	24	0.000004	-0.0073	-0.0098	3.9673	4.126			
26	25	4.16667E-06	-0.0098	-0.0122	3.9697	4.1284			

Value of time column
 = A2/6000000

Figure 2.23 SHPB data after modifying

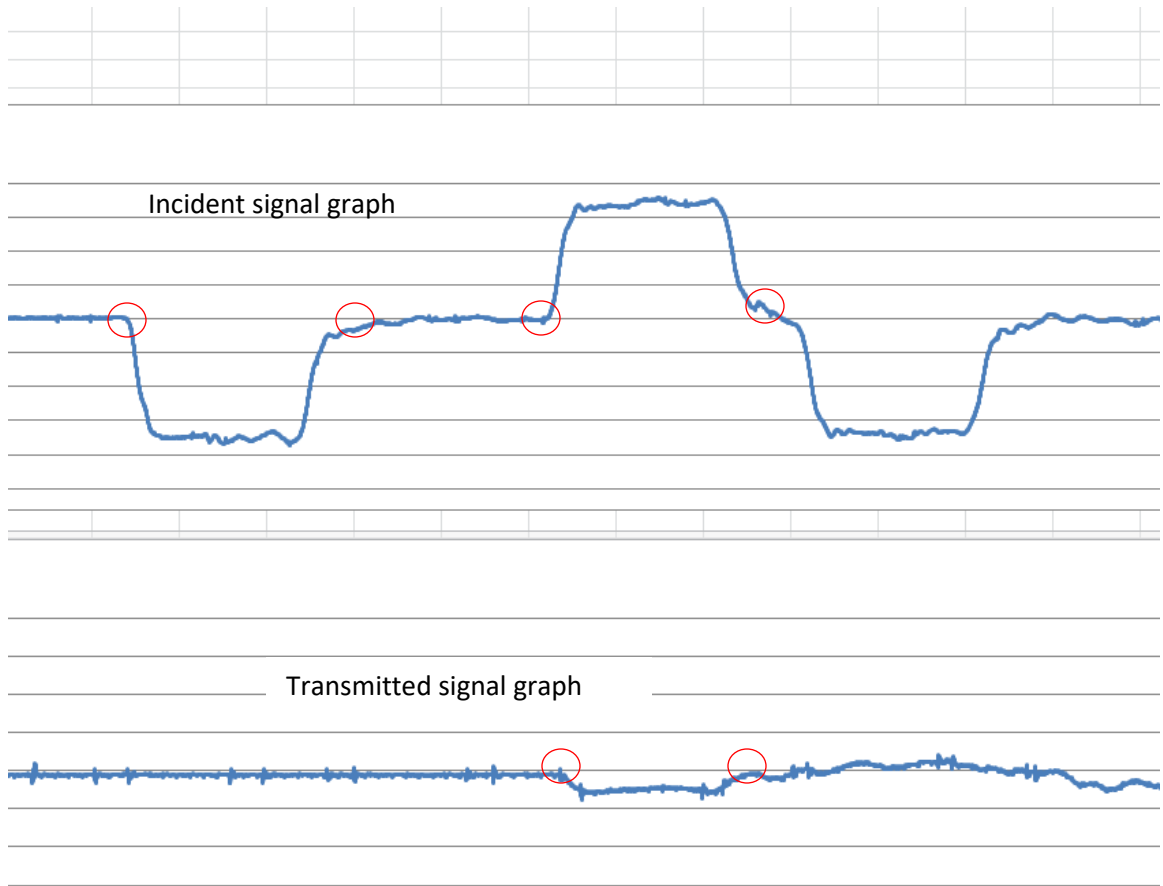


Figure 2.24 Incident and transmitted signal graphs

The starting and ending point of the required data are marked in Figure 2.24 for all three pulses. All the recorded data between these points are selected and put in an order of incident, transmitted and reflected pulse. The time values are changed from seconds to microseconds so that the final graphs from SHPB MATLAB file are versus microseconds. The four columns are then used as input data for the MATLAB program and the final graphs are obtained after corresponding correction factors are given as input for various strain rates.

CHAPTER THREE: HIGH STRAIN RATE PROPERTIES OF GRAPHENE REINFORCED ALUMINUM FOAMS AT ROOM TEMPERATURE

This chapter focusses on the high strain rate behavior of graphene reinforced aluminum foam at room temperature. The different concentrations of graphene reinforced foams used were: 0.2%, 0.4%, 0.5% and 0.62% by weight. Relative density of the foams used was 0.2 ± 0.01 . Compression tests were carried out at the strain rates of 1000, 1400, 1800 and 2200 s^{-1} .

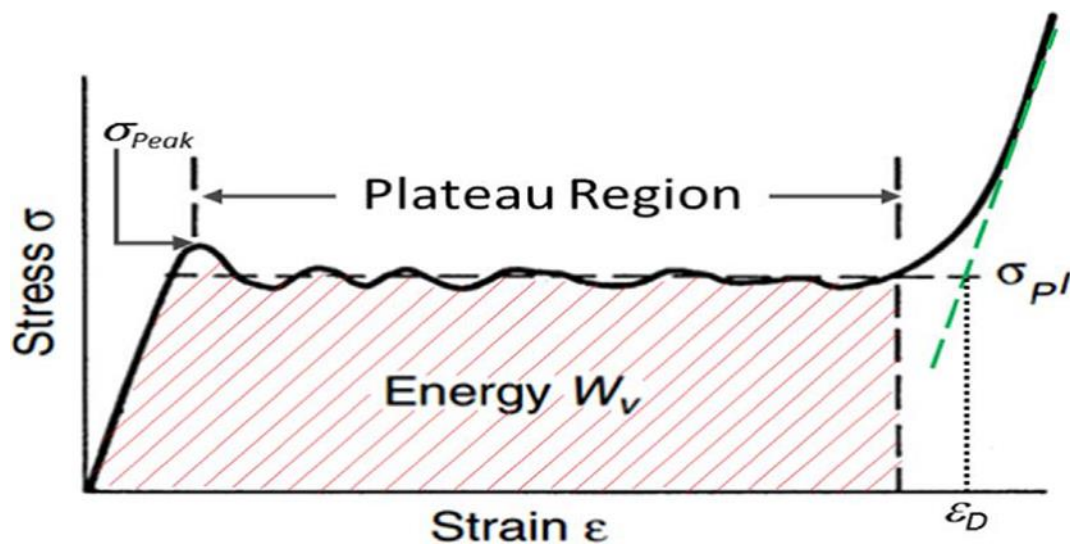


Figure 3.1 Typical compressive stress-strain behavior of aluminum foam

A typical response of aluminum foams that are under a compressive load is demonstrated in Figure 3.1 [48]. It is noticed that at low strain, aluminum foam displays linear elastic behavior until it reaches a peak stress. It indicates the start of plastic collapse in the foam. The next deformation region to follow this is known as plateau region. In this region the stress remains fairly constant and successive cell wall buckling and cell crushing takes

place throughout the region. The last deformation stage occurs when the material reaches the densification stage. In this, the stress rises considerably with strain. Energy absorption capacity appears to be a significant property of aluminum foam. The area under the stress-strain curve till the beginning of the densification region (shaded area in Figure 3.1) is defined as the energy absorbed per unit volume (W). The zigzag behavior in the stress-strain curves may be due to localized deformation of layer-by-layer collapse and compaction of cells [49].

Figures 3.2, 3.3, 3.4 and 3.5 presents the dynamics compressive stress-strain curves for 0.2, 0.4, 0.5 and 0.62 wt% graphene Al-foams at strain rates of 1000 s^{-1} , 1400 s^{-1} , 1800 s^{-1} and 2200 s^{-1} respectively. At a strain rate of 1000 s^{-1} (Figure 3.2), the maximum peak and plateau stress found were 11.16 MPa and 10.72 MPa respectively for 0.62 wt%. graphene aluminum foam. The 0.2% wt. graphene foam performed better than the 0.4 wt% graphene foam but is inferior when compared with the results obtained in 0.5 wt. % graphene.

The mechanical behavior of Al foams reinforced with graphene at a strain rate of 1400 s^{-1} is shown in Figure 3.3. It was noted that the peak stress of 12.98 MPa and plateau stress of 12.55 MPa are observed for the 0.62wt. % graphene concentration. The performance of 0.5 wt. % graphene concentration is better than that of 0.2 wt.% as well as 0.4 wt. % graphene foam.

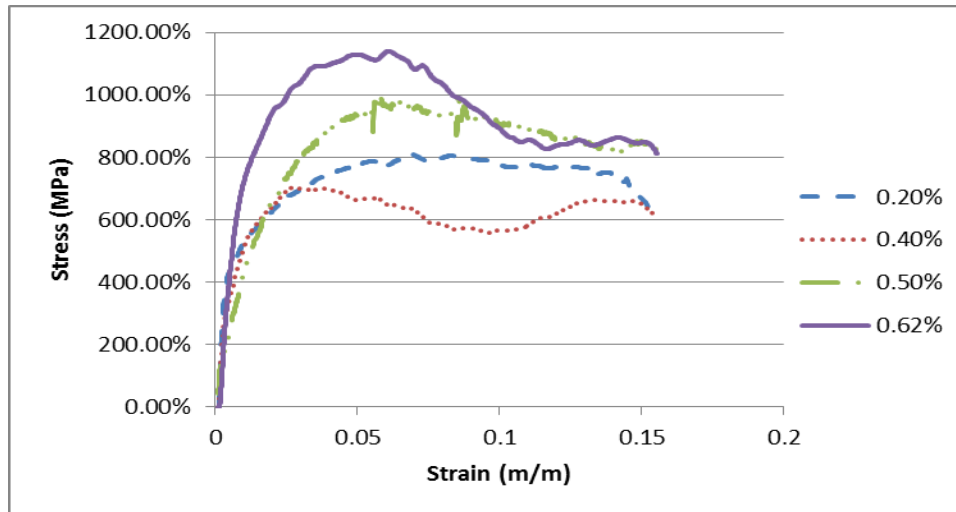


Figure 3.2 High strain rate (1000 s^{-1}) compressive stress-strain response for different graphene composition

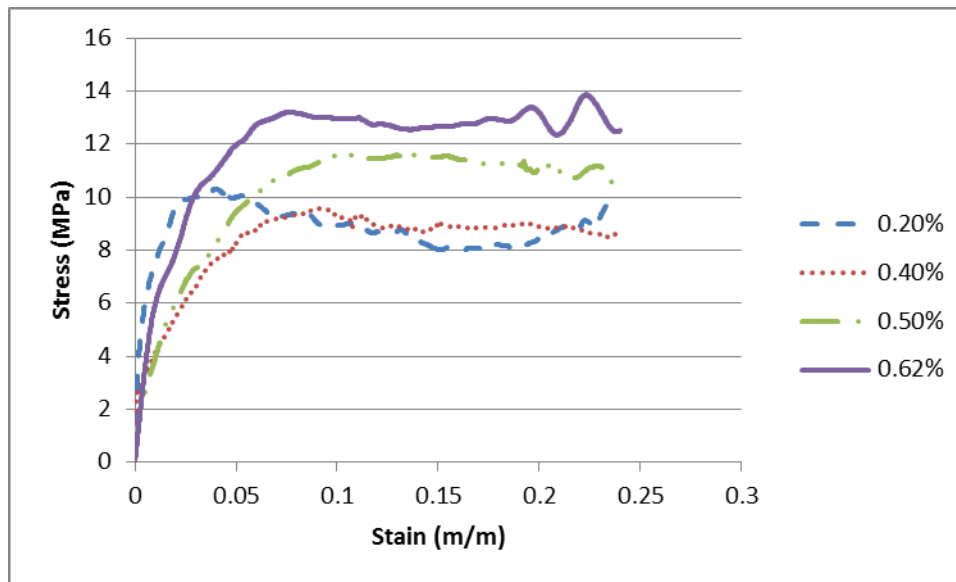


Figure 3.3 High strain rate (1400 s^{-1}) compressive stress-strain response for different graphene composition

Figure 3.4 depicts the stress-strain curve of 0.2, 0.4, 0.5 and 0.62% wt. graphene aluminum foams at the strain rate of 1800 s^{-1} . At this strain rate, the maximum peak stress and plateau stress are seen in 0.62 wt. % graphene concentration. The peak of 14.97 MPa and plateau stress of 13.50 MPa is observed for this type of foam.

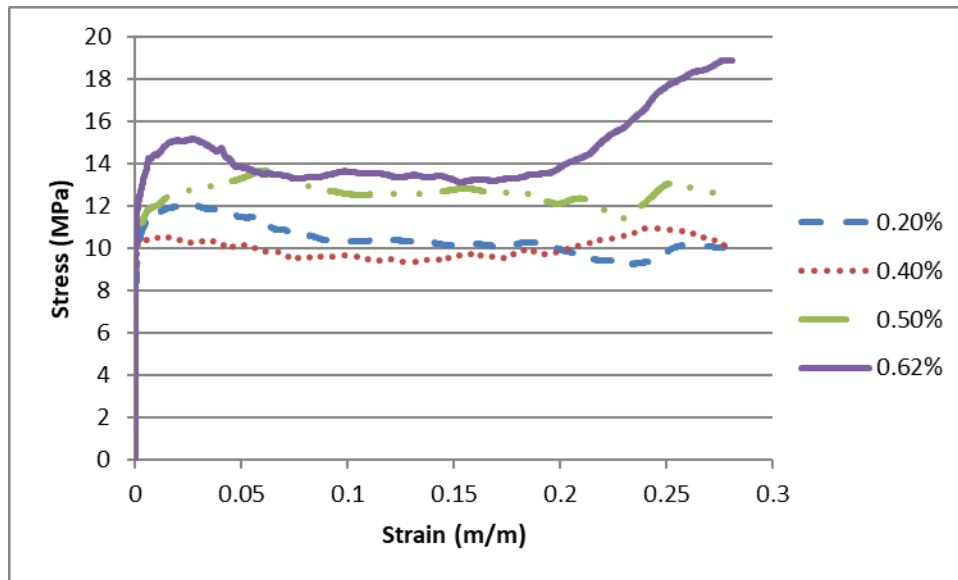


Figure 3.4 High strain rate (1800 s^{-1}) compressive stress-strain response for different graphene composition

The performance of graphene-reinforced foam at the strain rate of 2200 s^{-1} is shown in Figure.3.5. The maximum peak stress and plateau stress detected is 17.48 MPa and 18.82 MPa for the 0.62 wt. % graphene concentration which exceeded the values observed from the other three foam concentrations.

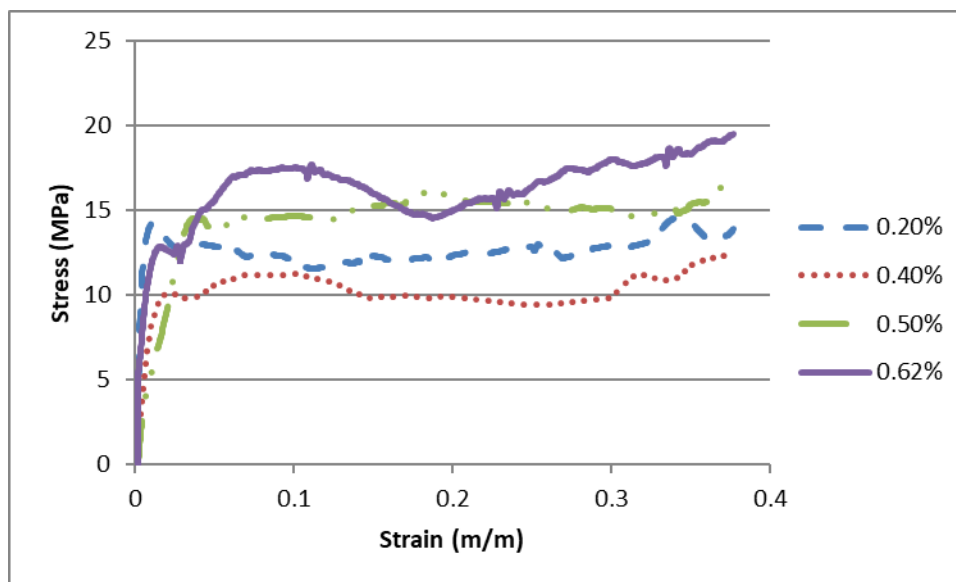


Figure 3.5 High strain rate (2200 s^{-1}) compressive stress-strain response for different graphene composition

The values of peak stress and plateau stress are presented in Table 3.1 in order to better visualize the result of varying strain rate on the compressive response of Al-foam. Three repeated experiments were performed at various strain rates at room temperature. Amongst the graphene concentrations studied the 0.62 wt. % foam displayed the maximum peak and plateau stress.

It was seen that with an increase in the strain rates, all graphene compositions showed an increase in the peak and plateau stress. The strain rates were varied from 1000 s^{-1} to about 2200 s^{-1} for all the foams. Under uniaxial compression, Al- foams are recognized to show

high-energy absorption capacity. Area under the stress-strain curve up to plateau strain is described as the energy absorption per unit volume (W) and is given by equation 1.

$$W = \int_0^{\varepsilon} \sigma(\varepsilon) d\varepsilon \quad (1)$$

Table 3.1 Peak and plateau stresses at different strain rates and graphene composition

Strain rate (s ⁻¹)		Foam type (wt.% graphene)			
		0.2	0.4	0.5	0.62
1000	σ_{Peak} (MPa)	8±0.6	7.01±0.54	9.88±0.24	11.16±0.32
	σ_{Plateau} (MPa)	7.5±0.35	5.59±0.62	9.05±0.45	10.72±0.67
1400	σ_{Peak} (MPa)	10.28±0.1	9.33±0.18	11.41±0.58	12.98±0.18
	σ_{Plateau} (MPa)	8±0.5	8.89±0.44	11±0.32	12.55±0.21
1800	σ_{Peak} (MPa)	12.54±0.44	10.28±0.19	13.35±0.12	14.97±0.08
	σ_{Plateau} (MPa)	10.36±0.79	9.31±0.35	12.58±0.23	13.50±0.12
2200	σ_{Peak} (MPa)	14.16±0.31	11.19±0.2	14.81±0.52	17.48±0.44
	σ_{Plateau} (MPa)	12.06±0.42	9.67±0.54	15.97±0.61	18.82±0.68

Energy absorption of 0.2, 0.4, 0.5 and 0.62 wt. % graphene has been evaluated for different strain rates. Plateau stress was calculated by taking the average stress of 15 points on the stress-strain curve after the peak stress while, energy absorption was calculated by multiplying the obtained plateau stress with strain. It can be seen that strain rate strongly influences the energy absorption (Figure 3.6). According to the Aldoshan *et.al* [49], the peak stress of unreinforced aluminum foam varies from 6.5 at a strain rate of 1300 s⁻¹ to 8 MPa at a strain rate of 2300 s⁻¹ and the plateau stress varies from 4.2 MPa

to 6.5 MPa for the same range of strain rate. Therefore the results of this study depicts that mechanical properties of aluminum foams reinforced with graphene has increased.

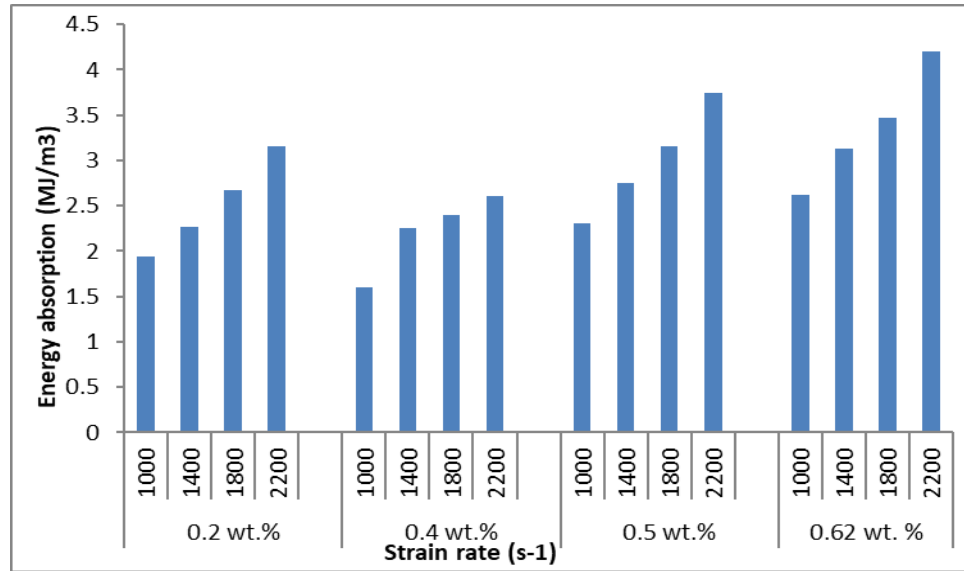
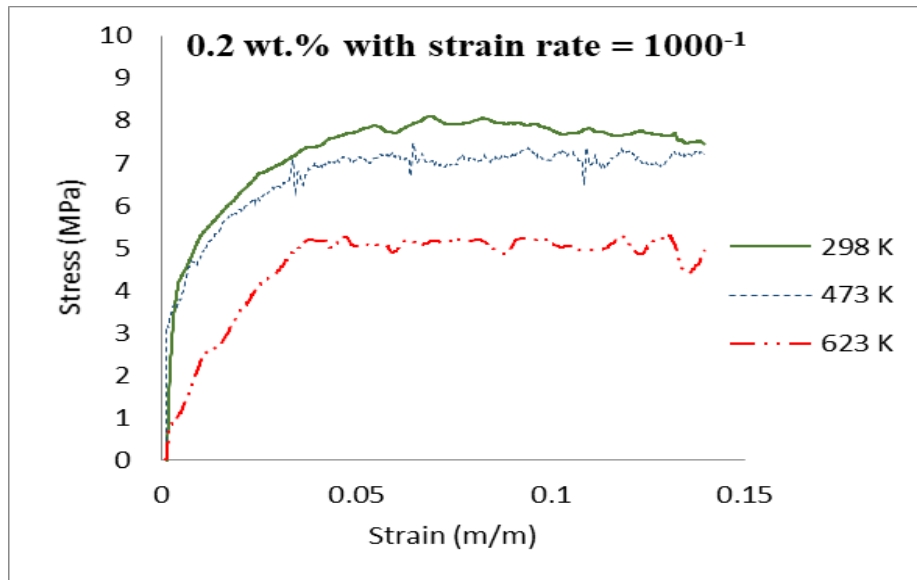


Figure 3.6 Energy absorption of aluminum foams as a function of strain rates

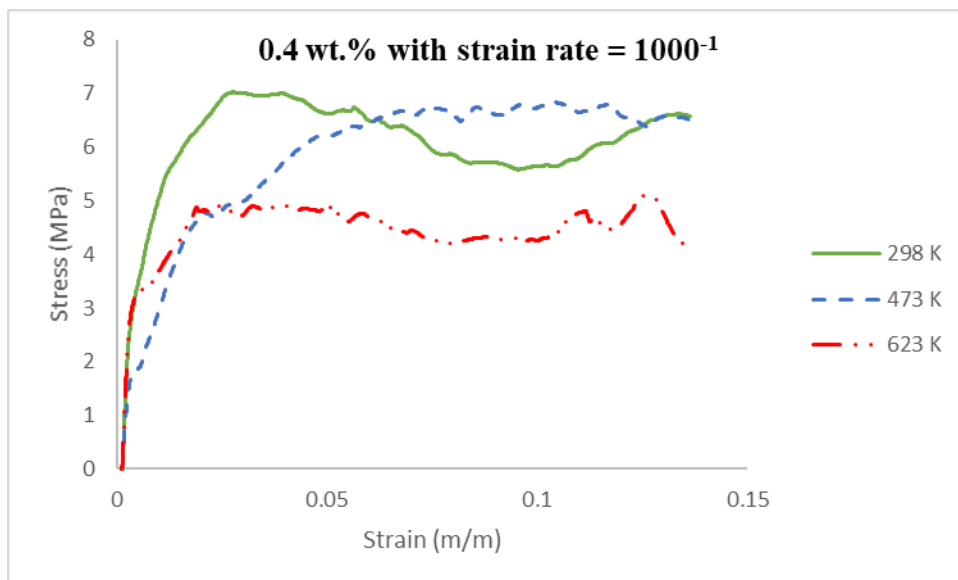
**CHAPTER FOUR: HIGH STRAIN RATE PROPERTIES
OF GRAPHENE REINFORCED ALUMINUM FOAMS
AT HIGH TEMPERATURE**

This chapter focusses on the high strain rate behavior of graphene reinforced aluminum foam at high temperature. Four different concentrations of graphene reinforced foams were used (0.2%, 0.4%, 0.5% and 0.62% by weight). Relative density of the foams used was 0.2 ± 0.01 . Compression tests were carried out at the strain rates of 1000, 1400, 1800 and 2200 s^{-1} . The temperatures at which the experiments were conducted were $150 \text{ }^{\circ}\text{C}$ (473 K) and $300 \text{ }^{\circ}\text{C}$ (623 K). Experimental results of closed cell Al-foam composites show that the dynamic mechanical properties in terms of peak stress and plateau stress increase as the strain rate increases under increasing temperatures. Amongst the different graphene concentrations studied, 0.62 wt% Al foam has the highest peak stress however it was 0.5 wt% Al foam that had the maximum plateau stress and energy absorption capacity under the range of temperature studied.

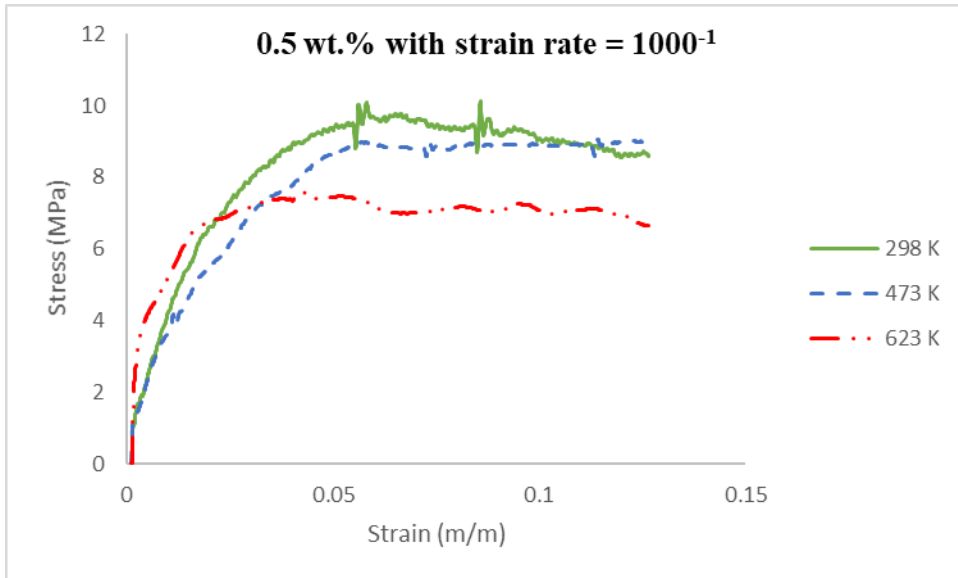
For a strain rate of 1000 s^{-1} (Figures 4.1 a-d), the highest peak stress observed are 10.62 MPa and 8.04 MPa at 473 K and 623 K respectively in the 0.62 wt.% concentration. Whereas, the highest plateau stress observed are 8.70 MPa and 7.12 MPa at 473 K and 623 K respectively in the 0.5 wt.% concentration.



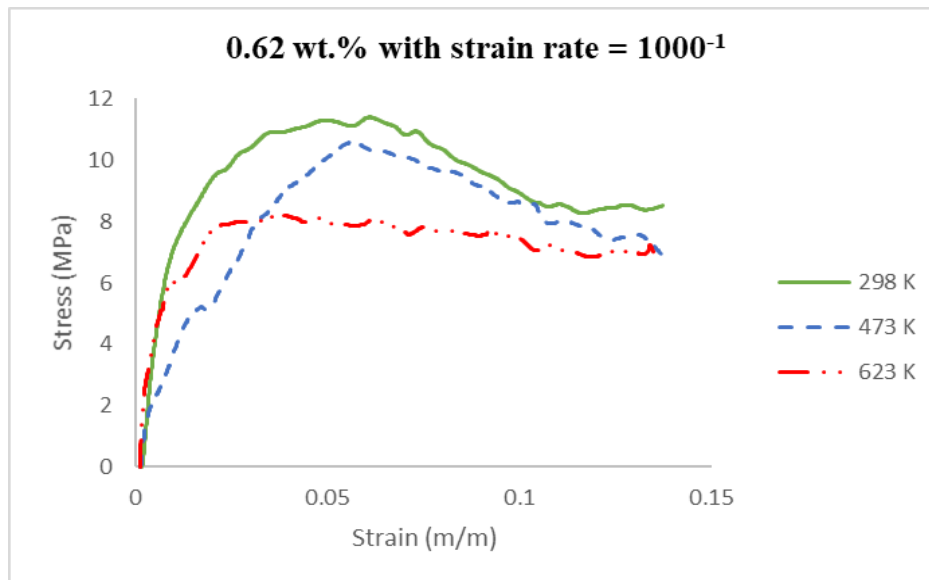
(a)



(b)



(c)

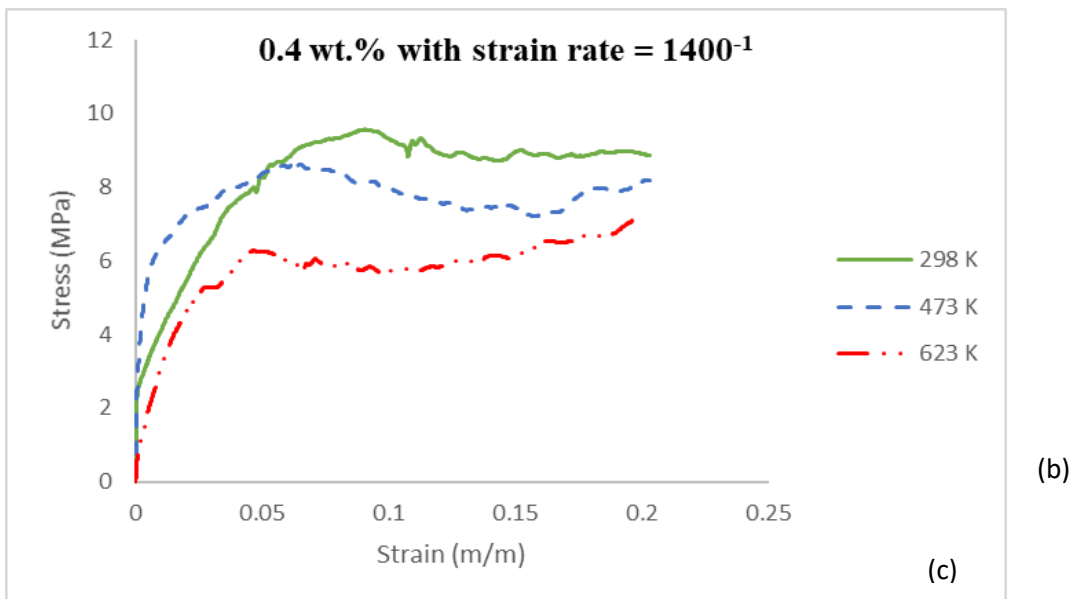
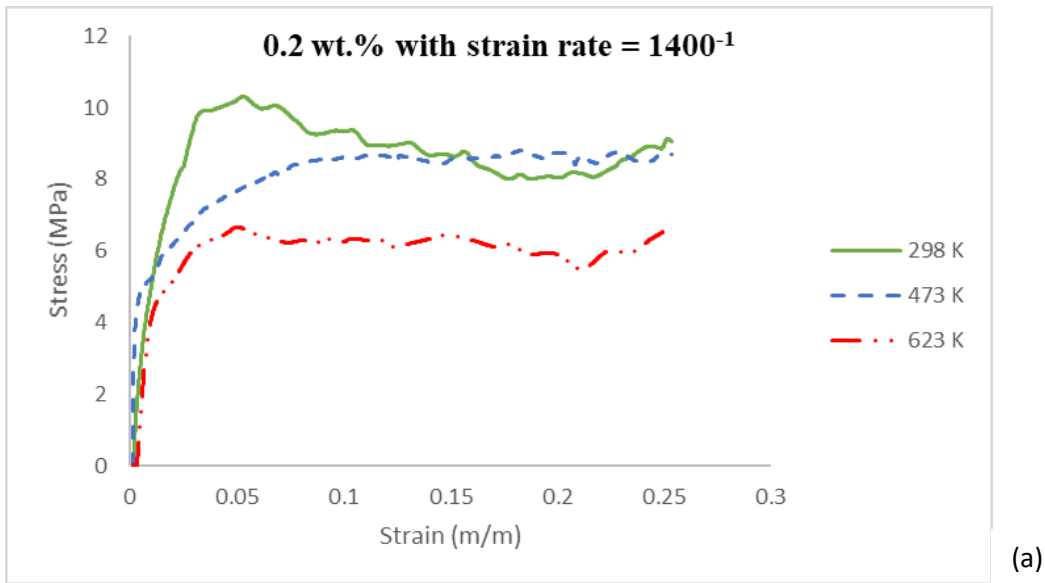


(d)

Figure 4.1 High strain rate (1000 s^{-1}) response of aluminum foams reinforced with various graphene compositions (a) 0.2 wt.%, (b) 0.4wt.%, (c) 0.5 wt.%, (d) 0.62 wt.%

The behavior of graphene reinforced aluminum foam at a strain rate of 1400 s^{-1} is shown in Figures 4.2 a-d. It is noted that at 473 K and 623 K, the highest peak stress of 10.55 MPa and 9.25 MPa respectively are observed for 0.62 wt.% concentration while the

highest plateau stress at these temperatures is noted at 0.5 wt.% concentration. At 473 the highest plateau stress is 9.40 MPa whereas for a temperature of 623 K the highest plateau stress is 8.16 MPa. The performance of 0.2 wt.% foam is similar of the 0.4 wt.% foam at high temperatures but displays better response at the room temperature.



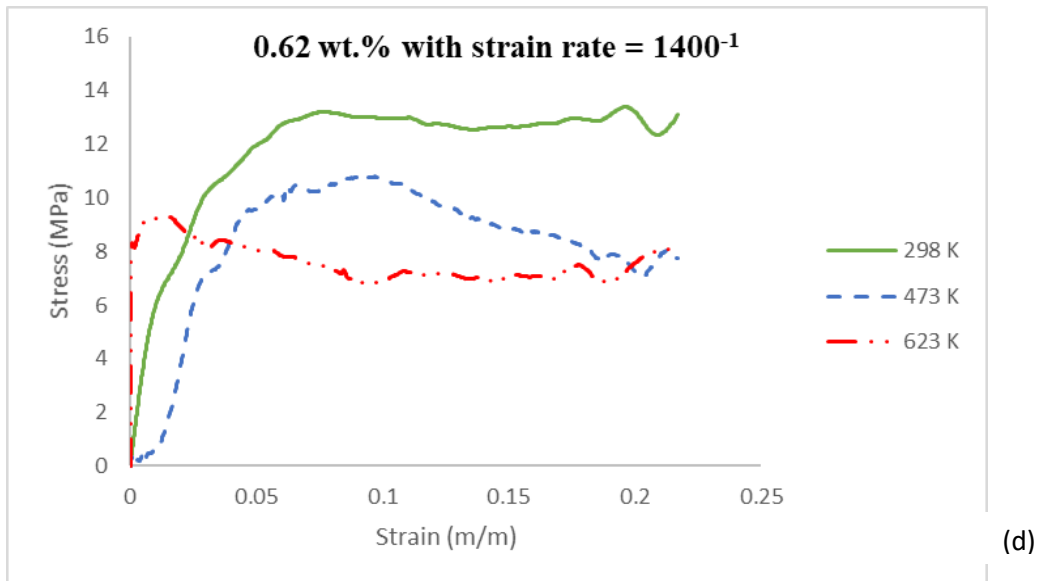
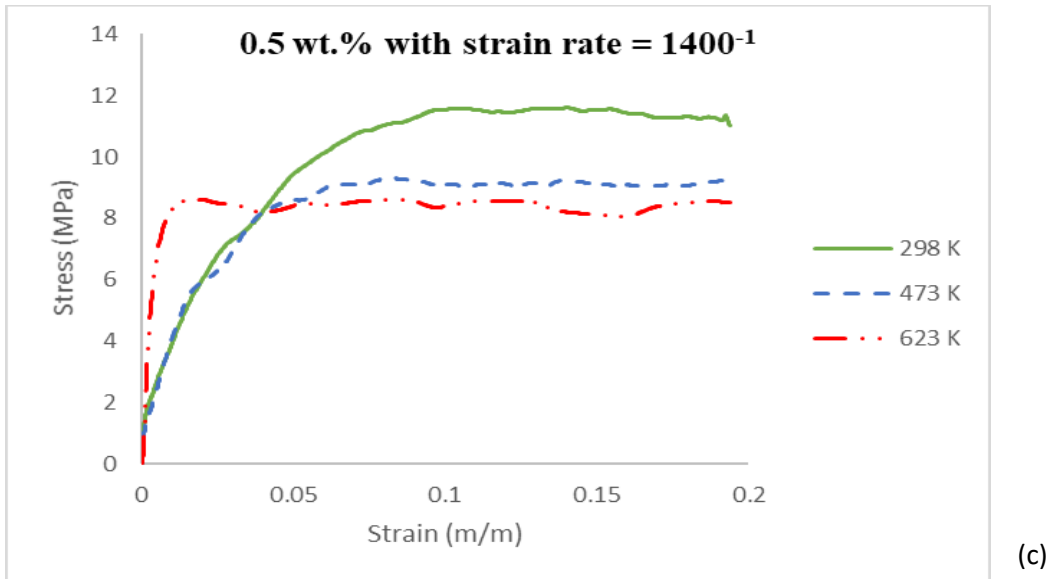
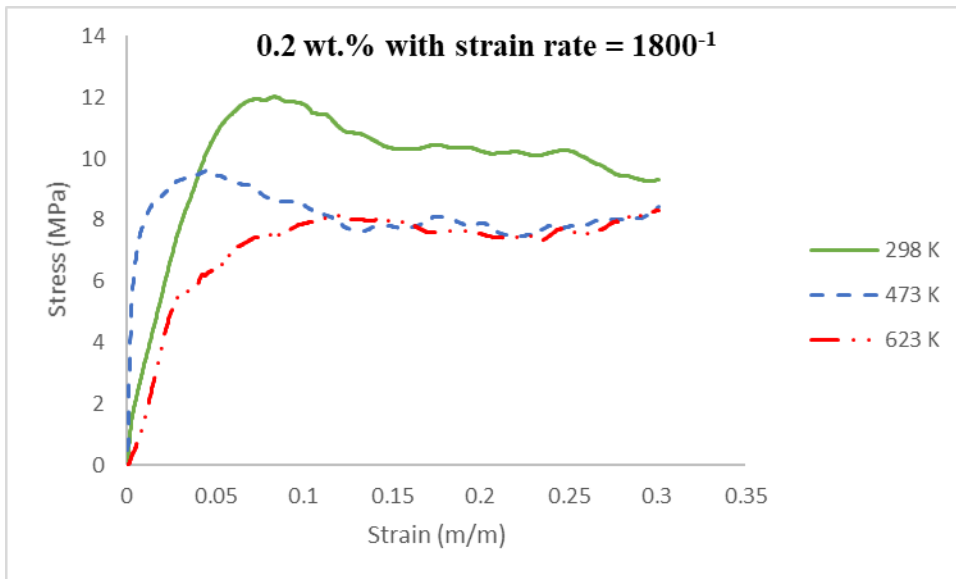
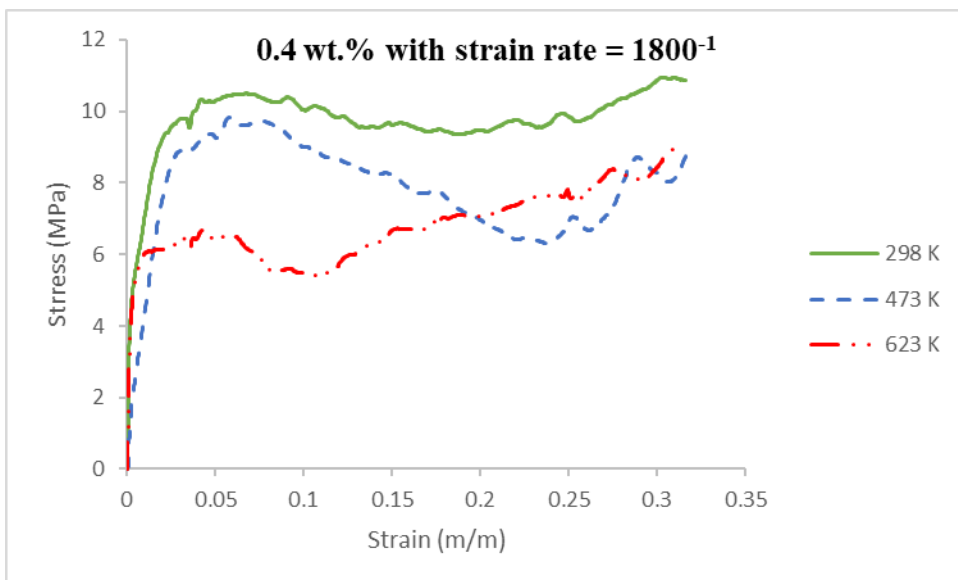


Figure 4.2 High strain rate (1400 s^{-1}) response of aluminum foams reinforced with various graphene compositions (a) 0.2 wt.%, (b) 0.4wt.%, (c) 0.5 wt.%, (d) 0.62 wt.%

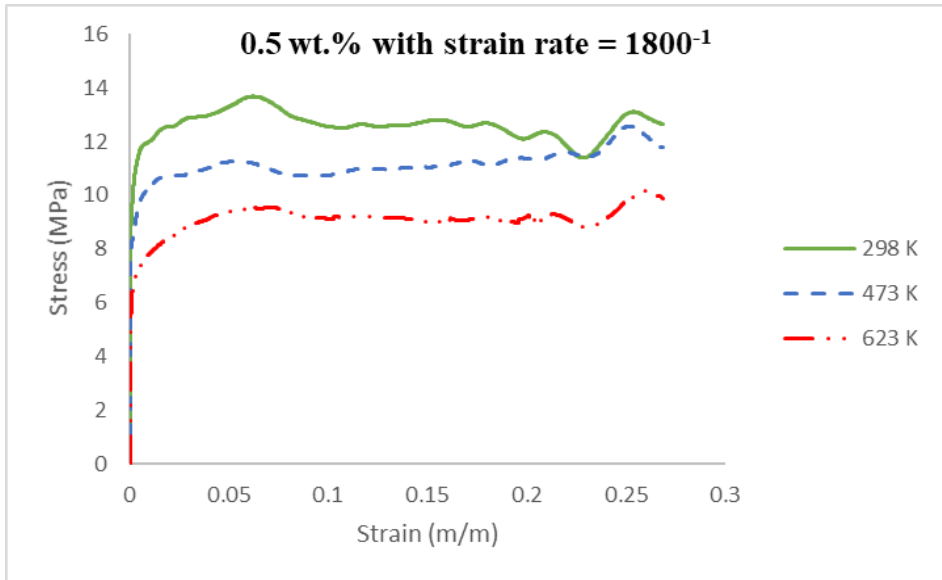
Figure 4.3 a-d presents all aluminum foams tested at 1800 s^{-1} and different temperatures. At this strain rate the maximum peak stress of 11.57 MPa and 10.01 MPa are observed for the 0.62 wt.% concentration at 473 K and 623 K respectively. The maximum plateau stress are observed for 0.5 wt.% concentration. For a temperature of 473 K the maximum plateau stress seen is 11.15 MPa while at 623 K the maximum plateau stress is noted as 9.13 MPa. Both the 0.2 wt.% and 0.4 wt.% show a very similar mechanical response at high temperature but lags the performance of 0.62 wt.% concentration foam.



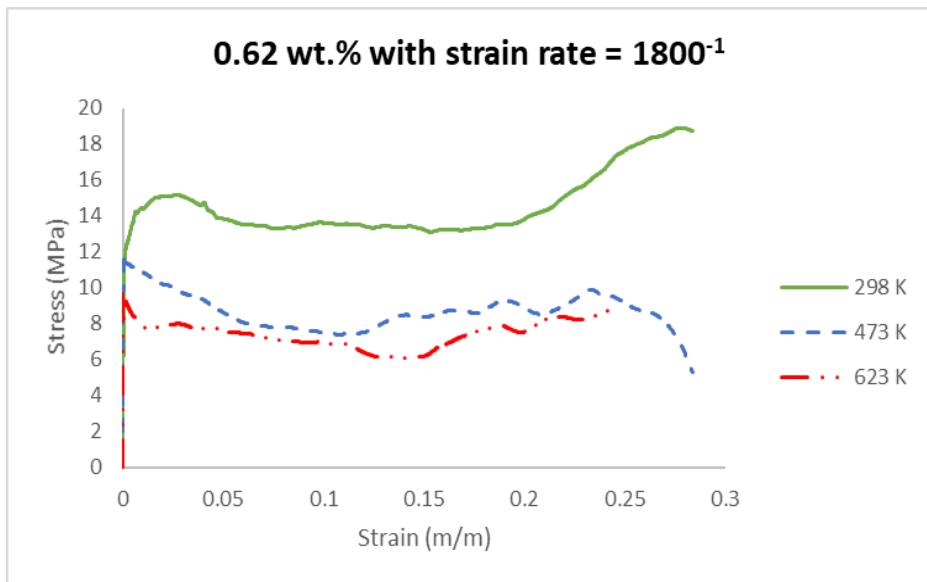
(a)



(b)



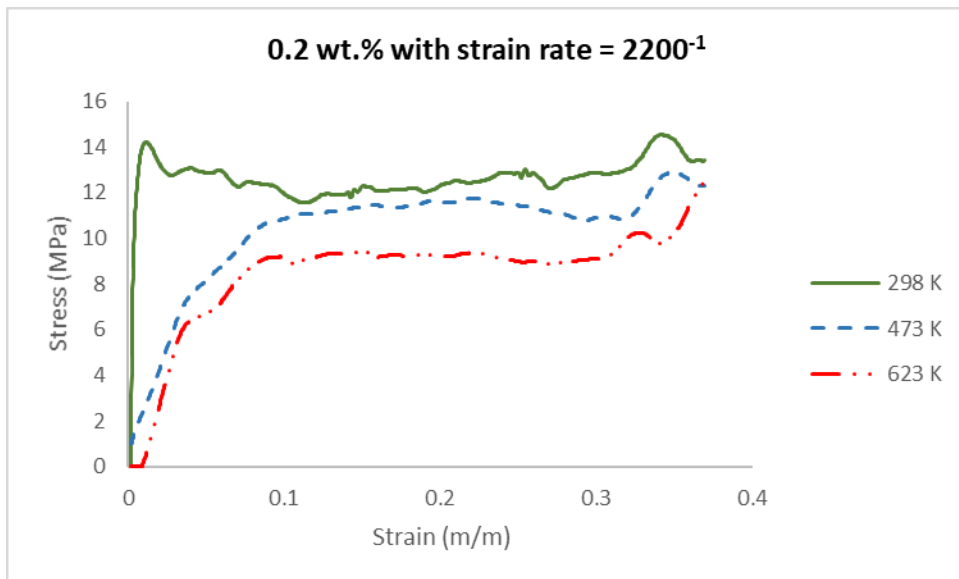
(c)



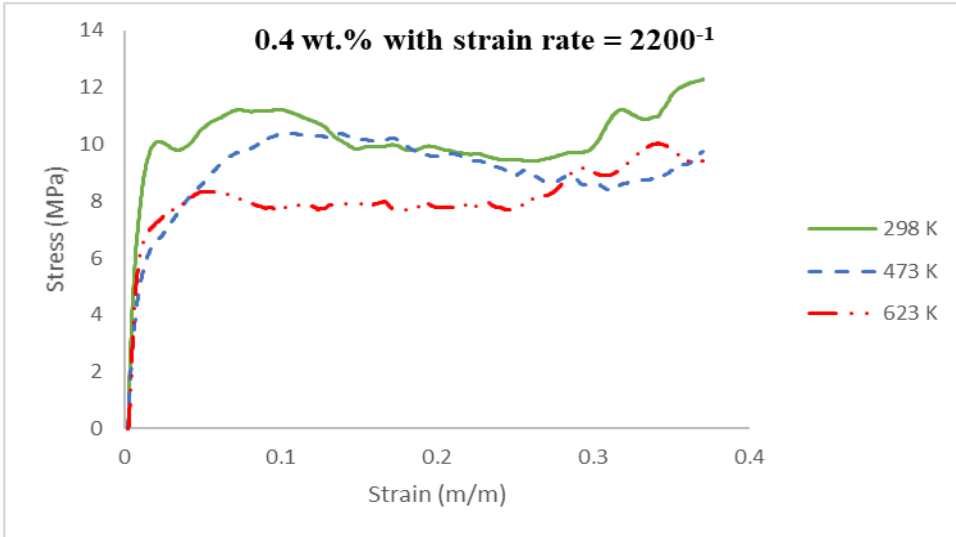
(d)

Figure 4.3 High strain rate (1800 s^{-1}) response of aluminum foams reinforced with various graphene compositions (a) 0.2 wt.%, (b) 0.4wt.%, (c) 0.5 wt.%, (d) 0.62 wt.%

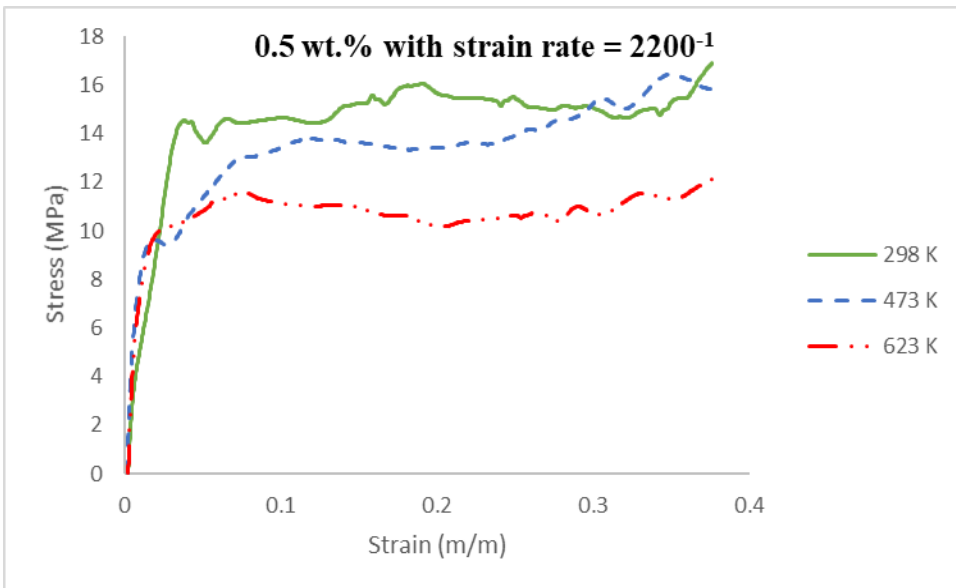
The mechanical responses of graphene reinforced aluminum foams for a strain rate of 2200s^{-1} are shown in Figures 4.4 a-d. The highest peak stress observed are 15.22 MPa and 12.72 MPa at 473 K and 623 K respectively in the 0.62 wt.% concentration. Whereas, the highest plateau stress observed are 12.31 MPa and 10.51 MPa at 473 K and 623 K respectively in the 0.5 wt.% concentration. The performance of 0.2 wt.% foam is comparable of the 0.4 wt.% foam at high temperatures but then again exhibits a better response at the room temperature.



(a)



(b)



(c)

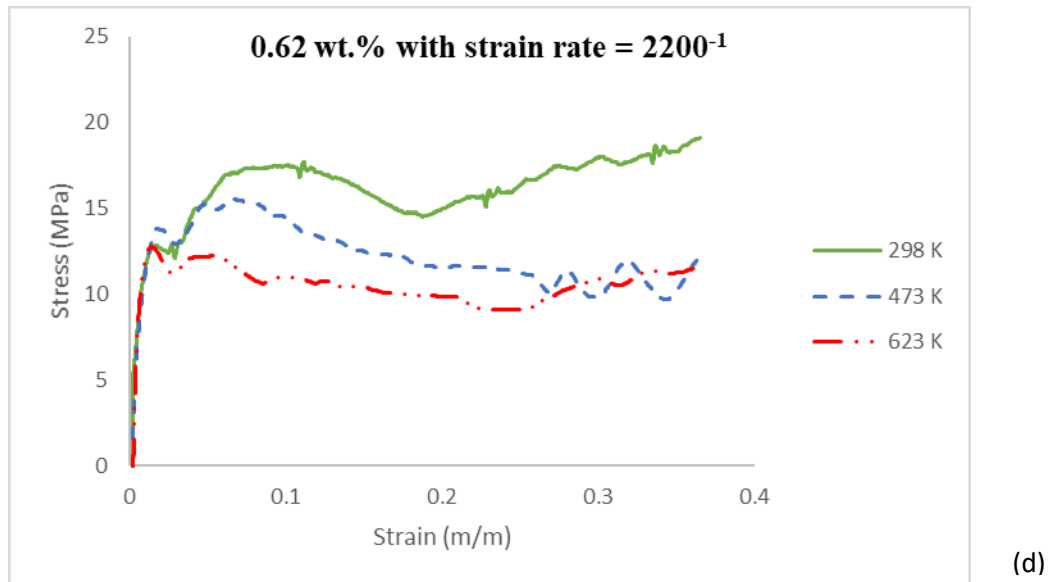


Figure 4.4 High strain rate (2200 s^{-1}) response of aluminum foams reinforced with various graphene compositions (a) 0.2 wt.%, (b) 0.4wt.%, (c) 0.5 wt.%, (d) 0.62 wt.%

The values of peak stress (Figure 4.5) and plateau stress (Figure 4.6) at 473 K and 623 K are presented in Table 4.1 and Table 4.2 respectively, in order to better visualize the result of varying strain rate on the compressive response of Al-foam. Three repeated experiments were performed at various strain rates at room temperature.

It is observed that for every graphene composition, the peak stress, plateau stress and energy absorbed (Figure 4.7) decreases with an increase in temperature from 298 K to 623 K. For every strain rate, the maximum peak stress, plateau stress and energy absorbed obtained at the three temperatures (298 K, 473 K and 623 K) studied is for 0.62 wt. % graphene reinforced aluminum foam. It is observed that amongst all the graphene

compositions studies, 0.2 wt. % had the lowest drop in the energy absorption capacity with an increase in temperature from 298 K to 623 K. Also, the values of these three parameters increase with an increase in the strain rate. It is seen that at 623 K, the stress rises rapidly and then we observe a nearly constant stress level or plateau stress. This behavior is very similar to an elastic-perfect plastic response

Table 4.1 Peak and plateau stresses at different strain rates and graphene composition at 473K

Strain rate (s ⁻¹)		Foam type (wt.% graphene)			
		0.2	0.4	0.5	0.62
1000	σ_{Peak} (MPa)	7.07±0.03	6.63±0.16	8.94±0.23	10.62±0.82
	σ_{Plateau} (MPa)	6.57±0.11	6.48±0.43	8.70±0.29	8.56±0.53
1400	σ_{Peak} (MPa)	9.03±0.11	8.32±0.36	9.55±0.34	10.55±0.24
	σ_{Plateau} (MPa)	8.73±0.14	7.98±0.28	9.40±0.31	8.94±0.50
1800	σ_{Peak} (MPa)	9.65±0.16	9.01±0.36	11.27±0.24	11.57±0.43
	σ_{Plateau} (MPa)	8.97±0.95	8.15±0.40	11.15±0.12	9.43±0.30
2200	σ_{Peak} (MPa)	12.35±0.27	9.78±0.60	13.46±0.11	15.22±0.23
	σ_{Plateau} (MPa)	11.78±0.44	8.9 ±0.03	12.31±0.9	12.54±0.38

Table 4.2 Peak and plateau stresses at different strain rates and graphene composition at 623 K

Strain rate (s ⁻¹)		Foam type (wt.% graphene)			
		0.2	0.4	0.5	0.62
1000	σ_{Peak} (MPa)	5.20±0.12	4.86±0.24	7.56±0.50	8.04±0.40
	σ_{Plateau} (MPa)	4.88±0.54	4.55±0.33	7.33±0.30	7.22±0.49
1400	σ_{Peak} (MPa)	6.61±0.21	6.08±0.41	8.61±0.08	9.25±0.51
	σ_{Plateau} (MPa)	6.12±0.14	5.74±0.35	8.16±0.19	7.64±0.43
1800	σ_{Peak} (MPa)	7.70±0.61	6.83±0.46	9.52±0.26	10.01±0.35
	σ_{Plateau} (MPa)	7.51±0.42	5.98±0.12	9.27±0.15	7.82±0.49
2200	σ_{Peak} (MPa)	9.18±0.11	8.78±0.31	11.60±0.27	12.72±0.54
	σ_{Plateau} (MPa)	9.02±0.12	7.56±0.35	10.62±0.21	10.07±0.65

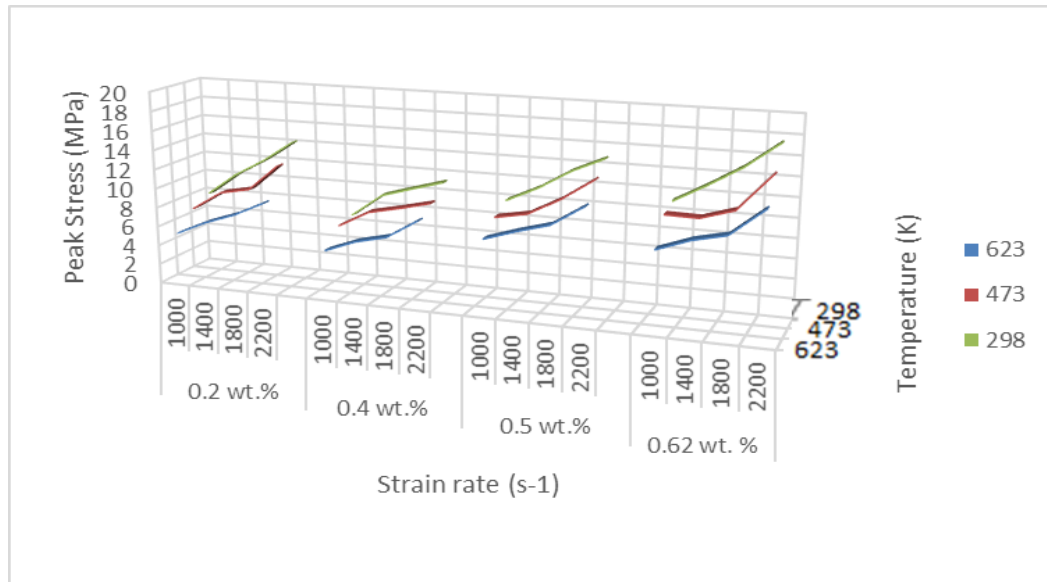


Figure 4.5 Values of peak stress for different compositions of graphene reinforced aluminum foam at different strain rates and temperatures

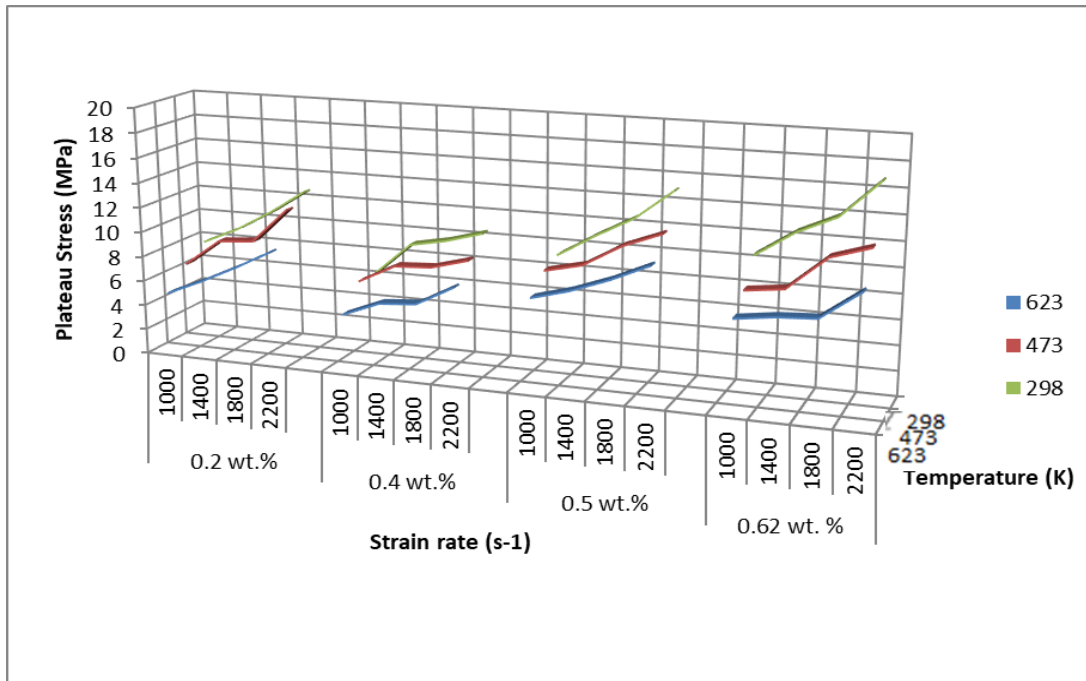


Figure 4.6 Values of plateau stress for different compositions of graphene reinforced aluminum foam at different strain rates and temperatures

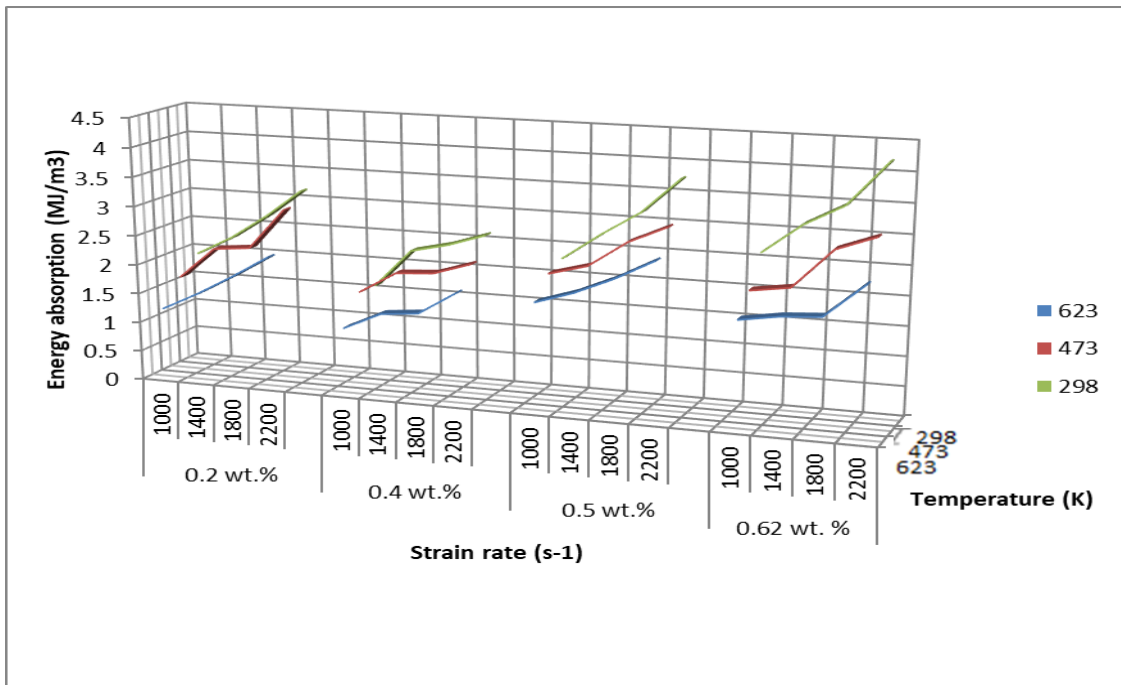


Figure 4.7 Values of energy absorption for different compositions of graphene reinforced aluminum foam at different strain rates and temperatures

CHAPTER FIVE: CONCLUSION

Split Pressure Hopkinson Bar system coupled with an infrared heater was used to determine the mechanical properties of graphene reinforced aluminum foams over varying temperatures and strain rates. The range of strain rate at which the study was conducted varied from 1000s^{-1} to 2200s^{-1} . It can be observed that the peak stress shows a strong dependence on strain rate for concentration of the foams. An increase in the value of peak stress can be seen as the strain rate is increased from 1000 s^{-1} to 2200 s^{-1} . A similar pattern is noted with the increase in plateau stress which is also dependent on strain rate.

It can be observed that the initial linearity which is analogous with the elastic region takes place at low strains of less than 0.03. Following that, the first peak detected in the stress-strain plot is known as peak stress. It suggests the start of the plastic collapse in the foam. Next region is known as the plateau region where under nearly constant stress, cell wall buckles and cell crushing occurs. Finally, the stage where the cells have collapsed through the whole cross-section is known as the densification stage.

- 1) It is noted that 0.62 wt.% shows the highest peak stress for all three temperatures studied. The peak stress improves slightly with an increase in the graphene concentration. The 0.4 wt. % graphene foam displayed the lowest peak stress

compared to all the different foam concentrations studied while 0.5 wt.% had a slightly higher peak stress than 0.2 wt.%.

- 2) It is found that there is a slight improvement in plateau stress with an increase in graphene concentration at 623 K. However, plateau stress is similar for 0.5 wt.% and 0.62 wt.%. The 0.4 wt.% graphene foam shows the lowest plateau stress among all the different foams studied. At room temperature and at 473 K, the highest plateau stress is noted for 0.5 wt.% as well as 0.62 wt. %.
- 3) At 623 K, the energy absorption improves marginally with increase in graphene concentration. However, for 0.5 wt.% and 0.62 wt.% the energy absorption is nearly the same. At 473 K and at room temperature, the 0.5 wt.% and 0.62 wt.% show the highest energy absorption. The 0.4 wt.% graphene foam displays the lowest energy absorption among all the different foams studied.
- 4) The 0.62 wt% graphene foam shows the highest strain rate sensitivity among all the foams studied.

REFERENCES

- [1] Meller, M. A., 1925, “Produit Métall. pour l’obtention d’objets Laminés,” p. 615.147.
- [2] Gibson, L. J., and Ashby, M. F., 1997, Cellular solids: Structure and Properties 2nd ed, UK Cambridge University Press, Cambridge.
- [3] Ashby, M. F., and Medalist, R. F. M., 1983, “The mechanical properties of cellular solids,” Metall. Trans. A, 14(9), pp. 1755–1769.
- [4] Bhat, B., and Wang, T. G., 1990, “A comparison of mechanical properties of some foams and honeycombs,” J. Mater. Sci., 25(12), pp. 5157–5162.
- [5] Simone, A. E., and Gibson, L. J., 1997, “Efficient structural components using porous metals,” Mater. Sci. Eng. A, 229(1-2), pp. 55–62.
- [6] Banhart, J., 2001, “Manufacture, characterisation and application of cellular metals and metal foams,” Prog. Mater. Sci., 46, pp. 559–632.
- [7] Andrews, E., Sanders, W., and Gibson, L. J., 1999, “Compressive and tensile behaviour of aluminum foams,” Mater. Sci. Eng. A, 270(2), pp. 113–124.
- [8] Banhart, J., 2013, “Light-Metal Foams-History of Innovation and Technological Challenges,” Adv. Eng. Mater., 15(3), pp. 82–111.
- [9] Hyunwoo Kim, Ahmed A. Abdala and Christopher W. Macosko, 2010 “Graphene/Polymer Nanocomposites”, Macromolecules, vol. 43, pp. 6515-6530

- [10] Xin Zhao, Qinghua Zhang and Dajun Chen, 2010, “Enhanced Mechanical properties of Graphene-based Poly(vinyl alcohol) Composites“, *Macromolecules*, vol. 43, pp. 2357-2363
- [11] Bertram Hopkinson, 1914 “A method of Measuring the Pressure produced in the Detonation of High Explosives or by the Impact of Bullets”, *Philosophical Transactions of the Royal Society of London, Series A*, vol. 213, pp. 437-456.
- [12] H. Kolsky, 1949 “An Investigation of the mechanical properties of Materials at very high rates of loading”, *Proc. Phys. Soc. (London)*, vol. 62B, pp. 676-700
- [13] Mukai, T., Kanahashi, H., Miyoshi, T., Mabuchi, M., Nieh, T. G., and Higashi, K., 1999, “Experimental study of energy absorption in a close-celled aluminum foam under dynamic loading,” *Scr. Mater.*, 40(8), pp. 921–927.
- [14] Zhao, H., Elnasri, I., and Abdennadher, S., 2005, “An experimental study on the behaviour under impact loading of metallic cellular materials,” *Int. J. Mech. Sci.*, 47(4-5 SPEC. ISS.), pp. 757–774.
- [15] D. J. Frew, M. J. Forrester and W. Chen, 2002, “Pulse shaping techniques for testing brittle materials with a Split Hopkinson Pressure bar”, *Experimental Mechanics*, vol. 42, No. 1, pp. 93-106
- [16] Hamada, T., Kanahashi, H., Miyoshi, T., and Kanetake, N., 2009, “Effects of the Strain Rate and Alloying on the Compression Characteristics of Closed Cell Aluminum Foams,” *Mater. Trans.*, 50(6), pp. 1418–1425.

- [17] G. T. Gray III, W. R. Blumenthal, C. P. Trujillo and R. W. Carpenter II, 1997, “Influence of Temperature and Strain rate on the Mechanical Behavior of Adiprene L-100”, *Journal de Physique IV*, vol. 7, pp. 523-528
- [18] W. Chen, B. Zhang and M. J. Forrestal, 1998, “A Split Hopkinson bar Technique for Low impedance Materials”, *Experimental Mechanics*, vol. 39, No. 2, pp. 81-85
- [19] Edwin Raj, R., Parameswaran, V., and Daniel, B. S. S., 2009, “Comparison of quasi-static and dynamic compression behavior of closed-cell aluminum foam,” *Mater. Sci. Eng. A*, 526(1-2), pp. 11–15.
- [20] Hakamada, M., Nomura, T., Yamada, Y., Chino, Y., Chen, Y., Kusuda, H., and Mabuchi, M., 2005, “Compressive Deformation Behavior at Elevated Temperatures in a Closed-Cell Aluminum Foam,” *Mater. Trans.*, 46(7), pp. 1677–1680.
- [21] Aly, M. S., 2007, “Behavior of closed cell aluminium foams upon compressive testing at elevated temperatures: Experimental results,” *Mater. Lett.*, 61(14–15), pp. 3138–3141.
- [22] Cady CM, Gray GT, Liu C, Lovato ML, Mukai T, 2009, “Compressive properties of a closed-cell aluminum foam as a function of strain rate and temperature”, *Mater Sci Eng A* 525(1–2) pp.1–6.
- [23] Wang, P., Xu, S., Li, Z., Yang, J., Zheng, H., and Hu, S., 2014, “Temperature effects on the mechanical behavior of aluminum foam under dynamic loading,” *Mater. Sci. Eng. A*, 599, pp. 174–179.

- [24] Seo, S., Min, O., and Yang, H., 2005, "Constitutive equation for Ti-6Al-4V at high temperatures measured using the SHPB technique," *Int. J. Impact Eng.*, 31(6), pp. 735–754.
- [25] Apostol, M., Vuoristo, T. and Kuokkala, V. T., 2003, "(High temperature high strain rate testing with a compressive SHPB," *J. Phys. IV*, 110(459–464).
- [26] Frantz, C. E., Follansbee, P. S. and Wright, W. T., 1984, "Experimental techniques with the split Hopkinson bar.," In: *Proceedings of the 8th International Conference on High Energy Rate, Fabrication, Texas*, pp. 229–236.
- [27] Banhart, J., Baumeister, J., and Weber, M., 1996, "Damping properties of aluminium foams," *Mater. Sci. Eng. A*, 205(1-2), pp. 221–228.
- [28] Liu, C. S., Zhu, Z. G., Han, F. S., and Banhart, J., 1998, "Internal friction of foamed aluminium in the range of acoustic frequencies," *J. Mater. Sci.*, 33(7), pp. 1769–1775.
- [29] Fuganti, B. A., and Lorenzi, L., 2000, "Aluminium Foam for Automotive Applications **," *Adv. Eng. Mater.*, (4), pp. 200–204.
- [30] Srinath, G., Vadiraj, A., Balachandran, G., Sahu, S. N., and Gokhale, A. A., 2010, "Characteristics of aluminium metal foam for automotive applications," *Trans. Indian Inst. Met.*, 63(5), pp. 765–772.
- [31] Stephani, G., Andersen, O., Quadbeck, P., and Kieback, B., 2010, "Cellular Metals for Functional Applications – an Overview," *PM2010 World Congr.*

- [32] GDA, 2014, “A high-speed train made of aluminium foam” [Online]. Available: <http://www.aluinfo.de/index.php/gda-news-en/items/a-high-speed-train-made-of-aluminium-foam.html>.
- [33] Jung, A., Lach, E. and Diebels, S., 2014, “New hybrid foam materials for impact protection,” *Int. J. Impact Eng.*, 64, pp. 30–38.
- [34] Crupi, V., Epasto, G., and Guglielmino, E., 2011, “Impact Response of Aluminum Foam Sandwiches for Light-Weight Ship Structures,” *Metals (Basel)*, 1(1), pp. 98–112.
- [35] Lefebvre, L. P., Banhart, J., and Dunand, D. C., 2008, “Porous metals and metallic foams: Current status and recent developments,” *Adv. Eng. Mater.*, 10(9), pp. 775–787.
- [36] Srivastava, V.C., 2007, “Processing, stabilization and applications of metallic foams,” *Materials science*, 25(3), pp.733-753
- [37] Marzbanrad, J. Keshavarzi, A., 2014, “ A numerical and experimental study on the crash behavior of the extruded aluminum crash box with elastic support”, *Latin American Journal of Solids and Structures*, 11(8), pp. 1329-1348.
- [38] D. A. Gorham, “A numerical method for the correction of dispersion in pressure bar signals”, *Journal of Physics E: Scientific Instruments*, vol. 16, pp. 477-479, 1983
- [39] Gama, B. A., Lopatnikov, S. L., and Gillespie, J. W., 2004, “Hopkinson bar experimental technique: A critical review,” *Appl. Mech. Rev.*, 57(4), p. 223.

- [40] Meyers, M., 1994, *Dynamic Behavior of Materials*, John Wiley & Sons, Inc.
- [41] W.Chen, W., and Song, B., 2011, *Spilt Hopkinson (Kolsky)Bar: Design, Testing and Applications*, Springer, New York.
- [42] Gray, G. T., 2000, “The Split Hopkinson Pressure Bar: An evolving quantification tool and technique for constitutive model validation,” *Mechanical Testing and Evaluation*: vol. 8, pp. 462–476.
- [43] Fu, B., Luo, H., Wang F., Churu G., Chu K.T., Hanan J.C., Sotiriou-Leventis C., Leventis N., Lu H., 2011, “ Simulation of the microstructural evolution of a polymer crosslinked templated silica aerogel under high strain rate compression”, *Journal of non-crystalline solids*, 357 (10), pp. 2063-2074.
- [44] Aldoshan A., Khanna S., 2017, “Dynamic High Temperature Compression of Carbon Nano Tube Reinforced Aluminum Foams”, *Journal of Dynamic Behavior of Materials*, 3(1), pp. 1-11.
- [45] Liu, H., Cao, Z. K., Luo, H. J., Shi, J. C., and Yao, G. C., 2013, “Performance of closed-cell aluminum foams subjected to impact loading,” *Mater. Sci. Eng. A*, 570, pp. 27–31.
- [46] Vecchio, K. S., and Jiang, F., 2007, “Improved Pulse Shaping to Achieve Constant Strain Rate and Stress Equilibrium in Split-Hopkinson Pressure Bar Testing,” *Metall. Mater. Trans. A*, 38(11), pp. 2655–2665.

- [47] Song, B., Nelson, K., Lipinski, R., Bignell, J., Ulrich, G., and George, E. P., 2014, “Dynamic high-temperature testing of an iridium alloy in compression at high-strain rates,” *Strain*, 50(6), pp. 539–546.
- [48] L.J. Gibson, Mechanical behavior of metallic foams, *Annu. Rev. Mater. Sci.* 30 (1), pp.191–227, 2000.
- [49] Aldoshan A, Khanna, S Effect of relative density on the dynamic compressive behavior of carbon nanotube reinforced aluminum foam, *Material Science and Engineering A* 689, pp.17-24,2017.
- [50] Mondal, D. P., Goel, M. D., and Das, S., 2009, “Compressive deformation and energy absorption characteristics of closed cell aluminum-fly ash particle composite foam,” *Mater. Sci. Eng. A*, 507(1-2), pp. 102–109.
- [51] Song, B., Nelson, K., Lipinski, R., Bignell, J., Ulrich, G., and George, E. P., 2014, “Dynamic high-temperature testing of an iridium alloy in compression at high-strain rates,” *Strain*, 50(6), pp. 539–546.

